frontiers in Chemistry

ORIGINAL RESEARCH
published: 11 April 2017
doi: 10.3389/fchem.2017.00024

Analogs of the Frog-skin Antimicrobial Peptide Temporin 1Tb Exhibit a Wider Spectrum of Activity and a Stronger Antibiofilm Potential as Compared to the Parental Peptide

Lucia Grassi[1], Giuseppantonio Maisetta[1], Giuseppe Maccari[2†], Semih Esin[1] and Giovanna Batoni[1]*

[1] Department of Translational Research and new Technologies in Medicine and Surgery, University of Pisa, Pisa, Italy, [2] Center for Nanotechnology Innovation @NEST, Italian Institute of Technology, Pisa, Italy

OPEN ACCESS

Edited by:
Neil Martin O'Brien-Simpson, University of Melbourne, Australia

Reviewed by:
David Andreu, Pompeu Fabra University, Spain
Minkui Luo, Memorial Sloan Kettering Cancer Center, USA

***Correspondence:**
Giovanna Batoni
giovanna.batoni@med.unipi.it

†Present Address:
Giuseppe Maccari, The Pirbright Institute, Pirbright, UK

Specialty section:
This article was submitted to Chemical Biology, a section of the journal Frontiers in Chemistry

Received: *22 December 2016*
Accepted: *23 March 2017*
Published: *11 April 2017*

Citation:
Grassi L, Maisetta G, Maccari G, Esin S and Batoni G (2017) Analogs of the Frog-skin Antimicrobial Peptide Temporin 1Tb Exhibit a Wider Spectrum of Activity and a Stronger Antibiofilm Potential as Compared to the Parental Peptide. Front. Chem. 5:24. doi: 10.3389/fchem.2017.00024

The frog skin-derived peptide Temporin 1Tb (TB) has gained increasing attention as novel antimicrobial agent for the treatment of antibiotic-resistant and/or biofilm-mediated infections. Nevertheless, such a peptide possesses a preferential spectrum of action against Gram-positive bacteria. In order to improve the therapeutic potential of TB, the present study evaluated the antibacterial and antibiofilm activities of two TB analogs against medically relevant bacterial species. Of the two analogs, TB_KKG6A has been previously described in the literature, while TB_L1FK is a new analog designed by us through statistical-based computational strategies. Both TB analogs displayed a faster and stronger bactericidal activity than the parental peptide, especially against Gram-negative bacteria in planktonic form. Differently from the parental peptide, TB_KKG6A and TB_L1FK were able to inhibit the formation of *Staphylococcus aureus* biofilms by more than 50% at 12 μM, while only TB_KKG6A prevented the formation of *Pseudomonas aeruginosa* biofilms at 24 μM. A marked antibiofilm activity against preformed biofilms of both bacterial species was observed for the two TB analogs when used in combination with EDTA. Analysis of synergism at the cellular level suggested that the antibiofilm activity exerted by the peptide-EDTA combinations against mature biofilms might be due mainly to a disaggregating effect on the extracellular matrix in the case of *S. aureus*, and to a direct activity on biofilm-embedded cells in the case of *P. aeruginosa*. Both analogs displayed a low hemolytic effect at the active concentrations and, overall, TB_L1FK resulted less cytotoxic toward mammalian cells. Collectively, the results obtained demonstrated that subtle changes in the primary sequence of TB may provide TB analogs that, used alone or in combination with adjuvant molecules such as EDTA, exhibit promising features against both planktonic and biofilm cells of medically relevant bacteria.

Keywords: Temporin 1Tb, analogs, biofilm, peptide design, antimicrobial peptides

INTRODUCTION

The development and rapid spread of antibiotic resistance among clinically relevant bacteria has dramatically reduced the effectiveness of antimicrobial therapies, thereby emerging as a major challenge for modern medicine (Boucher et al., 2009; Högberg et al., 2010). The ability of bacteria to form biofilms, architecturally complex cell aggregates embedded in an extracellular polymeric substance (EPS) and intrinsically tolerant to conventional antibiotics, further exacerbates the problem of bacterial resistance and is responsible for the persistence and chronicization of many types of infections (Costerton et al., 1999). Biofilms can be up to 1,000-fold more resistant to antimicrobial agents than their planktonic counterparts thanks to unique phenotypic and metabolic properties that allow them to implement resistance mechanisms at the community level. These include the presence of the EPS that reduces the diffusion of antibacterial compounds into the biofilm structure, the overall low growth rate of biofilm-forming bacteria, the presence of subpopulations of cells in a dormant state ("persisters"), and the cell proximity that promotes the horizontal gene transfer and the acquisition of mobile genetic elements encoding resistance (Høiby et al., 2010; Batoni et al., 2016a).

Over the last years, antimicrobial peptides (AMPs) have gained increasing attention as novel antimicrobial drugs for the control of infections sustained by antibiotic-resistant bacteria and/or bacterial biofilms. Due to their main mechanism of action, which involves the disruption of cell membrane integrity, AMPs exert a strong antimicrobial activity against a broad spectrum of pathogens, including multidrug-resistant bacterial strains, and generally prove a low frequency in inducing resistance (Zasloff, 2002). Moreover, they are able to target metabolically inactive and even non-growing cells that are commonly found within microbial biofilms (Di Luca et al., 2014; Batoni et al., 2016a). To date, over 2500 AMPs have been identified and evaluated for their antimicrobial activity (Antimicrobial Peptide Database: aps.unmc.edu/AP/main.php) and a growing number of them have also been tested against biofilms (BaAMPs database: www.baamps.it) (Di Luca et al., 2015).

The frog skin-derived peptide temporin 1Tb (TB) is considered a promising template for the development of next-generation antibiotics (Di Grazia et al., 2014). It is a 13-amino acid, mildly cationic (net charge +2) and α-helical peptide endowed with a bacterial membrane-perturbing activity (Mangoni et al., 2000). The peptide has previously demonstrated a fast and potent bactericidal action particularly against Gram-positive bacterial species, such as multidrug-resistant nosocomial strains of *Staphylococcus aureus* and *Enterococcus faecium* (Mangoni et al., 2008). The antibiofilm properties of TB have been also investigated showing high activity against both forming and mature biofilms of *Staphylococcus epidermidis*, especially when the peptide was used in combination with EDTA (Maisetta et al., 2016). Interestingly, it has been recently reported that the peptide is able to penetrate eukaryotic cells, kill intracellular *S. aureus* and promote wound-healing, further important properties in view of a therapeutic development (Di Grazia et al., 2014). Despite the many favorable features of TB, the preferential spectrum of activity of the peptide against Gram-positive bacteria partially limits its translatability into a clinically useful agent. The rational *in silico* design of novel peptides with optimized structural properties and the chemical manipulation of existing ones represent valid approaches to overcome the limitations of native peptides (Maccari et al., 2013). The introduction of appropriate changes in the peptide primary sequence and, thus, the alteration of crucial physicochemical parameters of AMPs (e.g., cationicity, hydrophobicity and amphipaticity) may significantly influence their bactericidal, cytotoxic and antibiofilm potential allowing to obtain molecules with improved antimicrobial efficacy and broader spectrum of action (Conlon et al., 2007; Takahashi et al., 2010; Batoni et al., 2016b). The aim of the present study was the optimization of TB activity against both planktonic bacteria and biofilms of medically relevant bacterial species. In particular, the antibacterial, antibiofilm and cytotoxic properties of TB were compared with those of two recently developed TB analogs. The first one (TB_KKG6A), described by Avitabile and co-workers, was initially obtained by Ala scanning on TB sequence and further optimized by increasing its positive charge (Avitabile et al., 2013). TB_KKG6A was found to efficiently interact with the lipopolysaccharide (LPS) of the Gram-negative bacterium *Escherichia coli* and to fold upon binding into a bent helix (Malgieri et al., 2015). The second one (TB_L1FK), firstly described in this study, was designed by us through statistical-based computational strategies (Maccari et al., 2013). Overall, TB analogs displayed a faster and stronger bactericidal activity than the parental peptide, especially against Gram-negative bacterial species in planktonic form. In addition, a marked antibiofilm activity against preformed biofilms of *S. aureus* and *Pseudomonas aeruginosa* was observed for both TB_KKG6A and TB_L1FK used in combination with EDTA, highlighting the potential of combinatorial drug therapies in the management of biofilm-related infections. When assayed on mammalian cells, TB_L1FK showed a lower cytotoxic activity against human epithelial cells as compared to TB_KKG6A, emerging as a promising molecule for the topical treatment of biofilm-associated infections.

Abbreviations: AMP, antimicrobial peptide; BPM, biofilm promoting medium; BSA, bovine serum albumin; CCS, combined consensus scale; MCC, Mathews correlation coefficient; MOEA, multi-objective evolutional algorithms; CFU, colony-forming units; CV, crystal violet; EDTA, ethylenediaminetetraacetic acid; EPS, extracellular polymeric substance; FCS, fetal calf serum; FIC, fractional inhibitory concentration; LPS, lipopolysaccharide; MBC, minimal bactericidal concentration; MIC, minimal inhibitory concentration; PBMCs, peripheral blood mononuclear cells; PBS, phosphate buffered saline; PI, propidium iodide; RBCs, red blood cells; SPB, sodium-phosphate buffer; TB, temporin 1Tb; TSA, tryptone soy agar; TSB, tryptone soy broth.

MATERIALS AND METHODS

Peptides

TB, TB_L1FK (designed as reported in "Results") and TB_KKG6A were synthesized by Proteogenix (Schiltigheim, France). Analysis of the synthetic peptides by high performance chromatography (HPLC) and mass spectrometry revealed purity

over 98%. Peptides were diluted in milli-Q water to obtain a stock solution of 1 mM and stored at −80°C. The main features of the peptides are shown in **Table 1**.

EDTA

Disodium ethylenediaminetetraacetic acid (EDTA) was purchased from Sigma-Aldrich (St. Louis, USA). A stock solution of EDTA (0.5 M) was prepared in milli-Q water by adjusting the pH to 8.0 with NaOH. The working solution (50 mM) was obtained by diluting the stock solution in milli-Q water, sterile filtered and stored at 4°C.

Bacterial Strains and Culture Conditions

The reference laboratory strains *Klebsiella pneumoniae* (ATCC BAA-1706), *P. aeruginosa* (ATCC 27853), *S. aureus* (ATCC 33591), and *S. epidermidis* (ATCC 35984) were used for the study. For the preparation of stock cultures, bacterial strains were grown in Tryptone Soy Broth (TSB) (Oxoid, Basingstoke, UK) until mid-log phase, subdivided in aliquots and stored at −80°C. For the colony-forming units (CFU) count, serially diluted bacterial suspensions were plated on Tryptone Soy Agar (TSA) (Oxoid) and incubated for 24 h at 37°C.

Bactericidal Activity and Killing Kinetics in Sodium-Phosphate Buffer

The bactericidal activity of TB, TB_L1FK and TB_KKG6A against *K. pneumoniae*, *P. aeruginosa*, *S. aureus*, and *S. epidermidis* was evaluated by the microdilution method in sodium-phosphate buffer (10 mM SPB, pH 7.4). Bacterial strains were grown in TSB until exponential phase and suspended in SPB to reach a density of 1×10^7 CFU/mL. A volume of 10 μL of the bacterial suspensions was added to 90 μL of SPB containing different concentrations of the peptides (from 1.5 to 48 μM). Bacteria suspended in SPB alone were used as cell viability control. Samples were incubated at 37°C with shaking for various times (5, 15, 30, 60, and 90 min), subsequently diluted 10-fold in TSB and plated on TSA to determine the number of CFU. The minimal bactericidal concentration (MBC) was defined as the minimal concentration of peptide causing a reduction of at least 3 Log_{10} in the number of viable bacteria after 90 min of incubation (Mangoni et al., 2008).

Biofilm Inhibition Assay

The ability of TB, TB_L1FK, and TB_KKG6A to prevent biofilm formation was evaluated against *S. aureus* and *P. aeruginosa*. Bacteria were grown overnight in TSB/Glc (TSB added with 0.25% (v/v) glucose) at 37°C. Stationary-phase cultures were diluted 1:1,000 in Biofilm Promoting Medium (BPM; TSB diluted 1:1 with 10 mM SPB at pH 7.4 and supplemented with 0.25% glucose). Bacterial suspensions were inoculated into flat-bottom polystyrene 96-well microplates (Corning Costar, Lowell, USA), in the absence (negative control) or in the presence of different concentrations of each peptide (from 12 to 48 μM). Microplates were incubated statically at 37°C for 24 h and biofilm biomass was estimated by crystal violet (CV) staining assay. To this aim, biofilms were rinsed three times with phosphate-buffer saline (PBS), air-dried for 15 min and incubated with 0.1% (w/v) CV (bioMérieux, Florence, Italy) for 15 min. The excess of CV was removed by washing the plates with PBS, while biofilm-associated CV was extracted with 98% ethanol (Sigma Aldrich) and quantified by measuring the optical density at 570 nm (OD_{570}) in a microplate reader (Model 550, Bio-Rad Laboratories Srl, Italy).

Biofilm Treatment Assay

The activity of TB, TB_L1FK, and TB_KKG6A against preformed (24-h old) biofilms of *S. aureus* and *P. aeruginosa* was also investigated. Briefly, biofilms were allowed to form for 24 h in flat-bottom 96-well microplates in the absence of antimicrobial compounds. Established biofilms were then washed three times with PBS in order to remove non-adherent cells and incubated in fresh BPM with different concentrations of the three peptides (from 15 to 120 μM). After 24 h of incubation, the viability of biofilm-associated cells was evaluated by CFU counting. For this purpose, biofilms were washed three times with PBS and bacterial cells were detached from the surface of the wells with a pipette tip, vigorously vortexed and plated in serial dilutions on TSA.

Evaluation of the Synergistic Effect between TB Analogs and EDTA on Preformed Biofilms

TB_L1FK and TB_KKG6A were combined with EDTA in order to enhance their activity against preformed biofilms of *S. aureus* and *P. aeruginosa*. To this aim, 24 h-old biofilms of the two bacterial species were exposed to different concentrations of the peptides (15 and 30 μM), alone and in combination with EDTA (1.25 and 2.5 mM). Microplates were incubated statically at 37°C for 24 h. Following incubation, the antibiofilm effect was evaluated in terms of number of biofilm-associated viable cells as previously described.

TABLE 1 | Main structural and physicochemical features of the peptides used in the study.

Peptide	Sequence	Molecular weight	Charge	Hydrophobicity[a]
TB	LLPIVGNLLKSLL-NH_2	1392.78	+2	3.62
TB_L1FK	**F**LPIVGLLKSLL**K**-NH_2	1440.86	+3	3.43
TB_KKG6A	**KK**LLPIV**A**NLLKSLL-NH_2	1663.15	+4	1.91

[a] *Hydrophobicity was calculated with the combined consensus scale (CCS) through the BaAMPs database (Di Luca et al., 2015).*

Evaluation of the Synergistic Effect Between TB Analogs and EDTA on Planktonic Bacteria in Biofilm-Like Conditions

The antibacterial activity of TB_L1FK and TB_KKG6A, used alone and in combination with EDTA, was also tested against planktonic cells of *S. aureus* and *P. aeruginosa*. The Minimal Inhibitory Concentration (MIC) of the peptides, EDTA and the peptide-EDTA combinations was determined by the microdilution method under the same experimental conditions used for the biofilm assay. Briefly, bacteria from overnight cultures were diluted 1:1,000 in BPM and incubated for 24 h at 37°C in propylene tubes in the presence of TB_L1FK and TB_KKG6A (from 3.75 to 120 μM), alone and combined with EDTA (from 0.3 to 10 mM). MIC was defined as the lowest concentration of the compounds resulting in the complete inhibition of visible growth. The effect of each combination on cell growth was studied using an adapted Fractional Inhibitory Concentration (FIC) index analysis. FIC index was calculated as follows: Σ ($FIC_A + FIC_B$), where FIC_A is the MIC of compound A in combination/MIC of compound A alone, and FIC_B is the MIC of compound B in combination/MIC of compound B alone. Synergism was defined as a FIC index ≤ 0.5, indifference as a FIC index > 0.5 and antagonism as a FIC index > 4 (Katragkou et al., 2015; Dosler et al., 2016).

Hemolysis Assay

Hemolytic activity of TB and its analogs was tested against human red blood cells (RBCs) as previously described (Tavanti et al., 2011). Briefly, peripheral blood obtained from healthy donors was centrifuged (1,000 × g for 10 min, 4°C) and washed three times with PBS (Euroclone, Milan, Italy). A suspension of RBCs (4%, v/v) was mixed with various concentrations of the peptides (from 12 to 96 μM) into a round-bottom polystyrene 96-well microplate (Corning Costar). RBCs suspended in PBS alone were used as negative control (0% hemolysis), while cells lysed with 0.1% Triton X-100 were taken as positive control (100% hemolysis). The microplate was incubated for 1 h at 37°C and then centrifuged at 1,000 × g for 20 min, 4°C. Supernatants were transferred to a new plate and the optical density at 450 nm (OD_{450}) was measured by means of a microplate reader. The hemolytic activity was quantified according to the following formula: hemolysis (%) = [($OD_{peptide} - OD_{negative\ control}$)/($OD_{positive\ control} - OD_{negative\ control}$)] × 100.

Cytotoxicity Assay

Cytotoxic activity of the peptides was assessed against human peripheral blood mononuclear cells (PBMCs) and human non-small-cell lung adenocarcinoma A549 cells (ATCC CCL-185).

PBMCs were isolated from buffy coats by conventional density gradient centrifugation. For this purpose, buffy coats were diluted 1:1 in PBS supplemented with 10% (v/v) sodium citrate (Sigma-Aldrich) and layered on Lympholyte-H gradient medium (Euroclone). Following centrifugation at 200 × g for 20 min at room temperature, the supernatant was eliminated in order to remove platelets. Buffy coats were further centrifuged at 800 × g for 20 min at room temperature and the lymphocyte/monocyte layer was harvested at the sample/medium interface. PBMCs were washed three times with PBS containing 0.5% (wt/v) bovine serum albumin (BSA; Sigma-Aldrich) and 10% sodium citrate, counted and re-suspended in RPMI 1640 (Euroclone) added with 10% (v/v) fetal calf serum (FCS; Euroclone) and 2 mM L-glutamine. Cells (1×10^5 per well) were seeded into round-bottom 96-well microplates (Corning Costar) and incubated with increasing concentrations of the peptides (from 12 to 96 μM) for 24 h at 37°C, 5% CO_2. PBMCs incubated with culture medium were used as negative (cell viability) control, while cells treated with cycloheximide (2 mg/mL) served as a positive (death) control.

A549 cells were grown in tissue culture flasks in Dulbecco's modified Eagle's medium (DMEM; Euroclone) containing 10% FCS and 2 mM L-glutamine. Confluent monolayers of A549 cells were washed with PBS, treated with a trypsin-EDTA solution (Sigma-Aldrich), centrifuged at 300 × g for 10 min, counted and re-suspended in complete DMEM at a final density of 5×10^4 cells/mL. A volume of 200 μL of the cell suspension was seeded into flat-bottom 96-well microplates (Corning Costar) and cultured for 24 h at 37°C, 5% CO_2. Peptides at a final concentration of 12–96 μM were added to the cells and incubated for further 24 h at 37°C, 5% CO_2. A549 cells incubated with culture medium were used as negative (cell viability) control, while cells treated with cycloheximide (2 mg/mL) served as a positive (death) control.

Cytotoxic activity was evaluated by the propidium iodide (PI) flow cytometric assay. To this end, PBMCs were washed once in PBS, resuspended in 100 μL, and incubated with 5 μL of a PI solution (50 μg/mL) (Sigma-Aldrich) for 4 min in the dark. Similarly, A549 cells were harvested by trypsinization, rinsed once with PBS and exposed to PI. Counting of viable (PI-negative) and dead (PI-positive) cells was carried out with a BD Accuri C6 flow cytometer (BD Biosciences, Mountain View, CA) and data were analyzed using BD Accuri C6 software (BD Biosciences). Cytotoxic effect was determined according to the following formula: Cytotoxicity (%) = [(PI-positive cells $_{peptide}$ – PI-positive cells $_{negative\ control}$)/(100 – PI-positive cells $_{negative\ control}$)] × 100. The IC_{50} values (Inhibitory Concentration) were defined as the concentration of the peptides causing 50% cell death as compared to the untreated control.

Statistical Analysis

All the experiments were performed at least in triplicate, unless otherwise specified. Differences between mean values of groups were evaluated by one-way analysis of variance (ANOVA) followed by Tukey-Kramer *post-hoc* test, after normalization of the data. A p-value < 0.05 was considered statistically significant.

RESULTS

TB_L1FK design

In order to improve the therapeutic potential of TB, a novel peptide was computationally designed starting from TB

sequence. In a previous work, chemophysical analysis of known AMPs sequences was successfully employed to design a statistical model of membrane-disrupting peptides able to account for non-natural amino acids (Maccari et al., 2013). In this work, an additional statistical model was designed to account for peptides' cytotoxic effect. Together with the previously described models for the secondary structure and the antimicrobial activity, a forth constraint was imposed in order to retain as much as possible the sequence similarity with TB. A dataset of peptides with proved cytotoxic effect was appositely designed by collecting and combining data from different bioactive peptide databases (Gupta et al., 2013). Furthermore, another set of peptides was designed to represent non-cytotoxic peptides, allowing the statistical model to grasp the features that distinguish the two sets (see Section 1.1 in the Supplementary Material). A number of filters aimed to normalize and uniform the training set of peptides were applied and then, sequences were encoded into physicochemical variables representing global and topological properties of peptides. A machine learning algorithm was adopted to build a prediction engine able to discern between toxic and non-toxic peptides (see the Supplementary Material for details in model training and validation). Model performance was evaluated by the Mathews Correlation Coefficient (MCC), which assesses the prediction in terms of true and false positives and negatives. In the final configuration, a prediction model with an MCC value of 0.82 was obtained. The candidate sequence, named TB_L1FK, was designed by applying the statistical model to a particular class of Genetic Algorithms, called Multi-Objective Evolutional Algorithms (MOEA) that allows to screen for candidates that simultaneously satisfy different criterions.

As reported in **Figure 1**, that shows a predictive simulation of the structure of TB and its two analogs, TB_L1FK displays similar physicochemical characteristics to the parental peptide. Hydrophobicity and net charge of TB_L1FK are close to those of TB, while TB_KKG6A presents a different hydrophobic profile and an increased net charge, particularly localized at the C-terminus. One of the aims in the computational design of TB_L1FK was to retain all the features that could infer in the membrane interaction of the peptide with the target cells. Besides, molecular hydrophobicity and net charge, as well as size and molecular weight, represent important aspects for the loading and the controlled release of peptides such as TB from nanostructured delivery systems (Piras et al., 2015).

Bactericidal Activity and Killing Kinetics of Peptides in Sodium-Phosphate Buffer

The antimicrobial activity of TB, TB_KKG6A, and TB_L1FK was evaluated in terms of MBC values toward *S. aureus* and *S. epidermidis* as models of Gram-positive bacteria and against *K. pneumoniae* and *P. aeruginosa* as models of Gram-negative bacteria. As shown in **Table 2**, TB was mainly active against Gram-positive bacteria and exhibited a bactericidal effect against Gram-negative bacteria only at 48 μM. Both analogs displayed a markedly increased activity compared to the parental peptide against all the bacterial species tested, but especially against the Gram-negative ones. In particular, a 2- to 8-fold reduction in the MBC compared to TB was observed against the Gram-positive bacteria, while an up to 16-fold decrease in the MBC value was observed in the case of the Gram-negative bacteria.

Time-kill studies on two representative bacterial species, *S. aureus* and *P. aeruginosa*, were carried out using the peptides at concentrations equal to their MBC. TB exerted its bactericidal activity toward *S. aureus* after approximately 90 min of incubation (**Figure 2A**). Both TB_L1FK and TB_KKG6A exhibited a faster killing kinetics than TB against the same bacterial species causing a reduction of at least 3 Log_{10} in the number of viable bacteria within 30 and 60 min, respectively (**Figure 2A**). All three peptides showed a more rapid bactericidal effect against *P. aeruginosa* than against *S. aureus* (**Figure 2B**). In particular, TB and TB_KKG6A showed similar killing kinetics, being bactericidal after 15 min of incubation, while the most rapid bactericidal effect was exerted by TB_L1FK that determined the complete eradication of the starting bacterial inoculum within as little as 5 min of incubation (**Figure 2B**).

Effect of TB and TB Analogs on Forming and Preformed Biofilms

We first investigated the ability of TB, TB_L1FK and TB_KKG6A to inhibit the formation of biofilms of *S. aureus* and *P. aeruginosa*, two bacterial species often involved in the formation of biofilms particularly refractory to antimicrobial treatment. The inhibitory effect was assessed by CV staining (total biofilm biomass) evaluating the percentage of biofilm formation after 24 h of incubation with TB or the two TB analogs, as compared to the control biofilms (cells incubated in medium only). As shown in **Figure 3A**, differently from the parental peptide, TB_L1FK and TB_KKG6A reduced the ability of *S. aureus* to form biofilm of more than 50% as compared to the untreated control at 12 μM. All the peptides caused around 80% decrease of the biofilm biomass at the concentration of 24 μM. When the peptides were assayed against forming biofilms of *P. aeruginosa*, no inhibitory activity of TB and TB_L1FK was observed at concentrations up to 48 μM (**Figure 3B**). In contrast, TB_KKG6A displayed a considerable ability in reducing the biomass of *P. aeruginosa* biofilms, causing an 80% inhibition at the concentration of 24 μM (**Figure 3B**).

Secondly, the efficacy of TB and its analogs against preformed (24 h-old) biofilms of *S. aureus* and *P. aeruginosa* was evaluated by CFU counting after 24 h of incubation with the peptides. In the case of *S. aureus* biofilms, TB did not exert a considerable antibiofilm activity at concentrations up to 120 μM (data not shown), while TB_L1FK and TB_KKG6A caused a decrease of approximately 2 Log_{10} in the number of biofilm-associated viable cells as compared to untreated biofilms at 30 μM (**Figures 4A,B**). When tested against biofilms of *P. aeruginosa*, none of the three peptides displayed a significant ability to reduce the number of CFU at the highest tested concentration (120 μM) (data not shown).

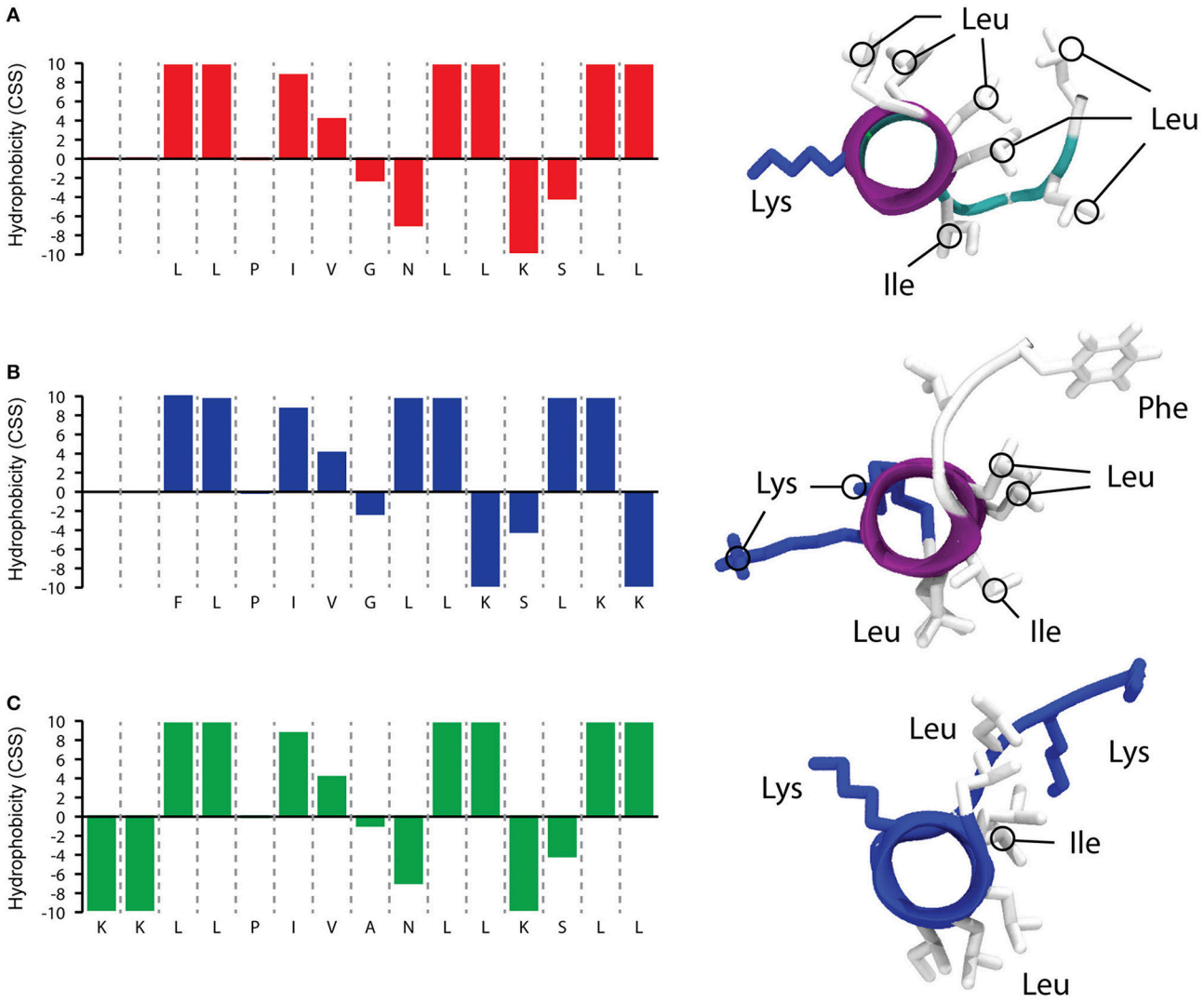

FIGURE 1 | Predictive simulations of hydrophobic profile and 3D structure of TB (A), TB_L1FK **(B)**, and TB_KKG6A **(C)**. The hydrophobic profile calculated with the combined consensus scale (CCS) is schematized on the left side (Maccari et al., 2013). 3D structures (right side of the figure) were calculated with PEP-FOLD3 (Lamiable et al., 2016); the distribution of hydrophobic and charged residues is highlighted.

Effect of TB Analogs, alone and in Combination with EDTA, on Preformed Biofilms

The possibility to improve the activity of TB analogs against preformed biofilms of *S. aureus* and *P. aeruginosa* was investigated combining the peptides with EDTA, a chelating agent previously reported to enhance the antibiofilm properties of TB (Maisetta et al., 2016). Indeed, the ability of EDTA to establish strong complexes with divalent cations essential for matrix stability could produce a matrix-disaggregating effect and promote the accessibility of peptides to biofilm-forming cells. The antibiofilm activity of various peptide-EDTA combinations was evaluated by CFU counting. Among all the tested combinations, the most powerful potentiating effect in terms of viable count reduction was obtained using both peptides at the concentration of 30 μM in combination with 1.25 mM (for *S. aureus*) or 2.5 mM EDTA (for *P. aeruginosa*). As regards *S. aureus* (**Figures 4A,B**), the combination of both TB_L1FK and TB_KKG6A with EDTA caused a reduction in the CFU number of approximately 1 Log_{10} (90%) compared to the peptides and EDTA used alone, and 3 Log_{10} (99.9%) compared to control biofilms after 24 h of incubation. Also in the case of *P. aeruginosa*, an enhanced ability of TB_L1FK and TB_KKG6A in biofilm reduction was demonstrated when peptides were used in combination with EDTA. Indeed, both peptide-EDTA combinations reduced the CFU number of

TABLE 2 | MBCs of TB, TB_L1FK, and TB_KKG6A against Gram-positive and Gram-negative bacteria in sodium-phosphate buffer (10 mM SPB, pH 7.4).

	Gram-positive		Gram-negative	
	S. aureus **ATCC 33591**	***S. epidermidis*** **ATCC 35984**	***K. pneumoniae*** **ATCC BAA-1706**	***P. aeruginosa*** **ATCC 27853**
TB	12[a]	6	48	48
TB_L1FK	6	1.5	6	6
TB_KKG6A	1.5	1.5	3	3

[a]*Numbers represent the MBC values expressed in μM.*

approximately 1 Log_{10} as compared to the peptide used alone (**Figures 4C,D**).

Effect of TB Analogs, alone and in Combination with EDTA, on Planktonic Bacteria in Biofilm-Like Conditions

In order to investigate whether the synergism between TB analogs and EDTA was due to a disaggregating effect on biofilm extracellular matrix and/or to a direct effect on bacterial cells, we assessed the activity of the combination on planktonic bacteria in biofilm-like conditions (i.e., stationary phase cells suspended in BPM) in terms of MIC values. As shown in **Table 3**, when tested alone, TB_L1FK displayed MICs of 15 and 120 μM against *S. aureus* and *P. aeruginosa*, respectively. In the case of TB_KKG6A, the growth-inhibiting effect was recorded at 7.5 μM for *S. aureus* and at 30 μM for *P. aeruginosa*. In order to identify any synergistic interaction, sub-inhibitory concentrations of each peptide and EDTA were combined and the FIC index for the different peptide-EDTA combinations was calculated. Differently to what observed for the biofilm mode of growth, EDTA was not able to potentiate the antibacterial activity of TB_L1FK and TB_KKG6A against planktonic cells of *S. aureus* (FIC index > 0.5, **Table 3**). Conversely, a synergistic effect between both TB analogs and EDTA was observed against *P. aeruginosa* planktonic cultures (FIC index $= 0.25$, **Table 3**). Interestingly, the combination with EDTA produced an 8-fold decrease in the MIC of both peptides against planktonic *P. aeruginosa* grown in biofilm-like conditions, suggesting a direct effect of EDTA in displacing divalent cations that are required for the integrity of the outer membrane of Gram-negative bacteria (Gray and Wilkinson, 1965; Asbell and Eagon, 1966).

Hemolytic Activity

The hemolytic activity of TB and TB analogs was evaluated toward human RBCs. As shown in **Figure 5**, no hemolytic effect of the parental peptide was assessed at concentrations up to 96 μM. An overall increase in hemolytic activity of both analogs was observed. Nevertheless, a hemolysis below 10%, commonly recognized as a safe cut-off (Amin and Dannenfelser, 2006), was observed at concentrations up to 24 μM of TB_KKG6A and up to 48 μM of TB_L1FK.

Cytotoxicity against PBMCs and A549 Cells

TB, TB_L1FK and TB_KKG6A were tested for cytotoxic activity on PBMCs and A549 cells by flow cytometric determination of PI incorporation in cells treated with different concentrations of the three peptides. As shown in **Figure 6**, TB did not exhibit a significant cytotoxic effect toward both PBMCs and A549 cells at any of the tested concentrations. Indeed, an approximately 90% viability was observed at 96 μM for both cell types. Both TB analogs displayed higher cytotoxicity against both cell types as compared to TB (**Figures 6A,B**). When the toxic effect was evaluated as IC_{50} value, TB_L1FK and TB_KKG6A showed comparable levels of cytotoxicity against PBMCs (IC_{50} values of 52 and 49 μM, respectively). In contrast, TB_L1FK displayed lower levels of cytotoxicity against A549 cells with an IC_{50} value of 59 vs. 16 μM of TB_KKG6A.

DISCUSSION

The use of AMPs as an alternative to conventional antimicrobial agents in the treatment of antibiotic-resistant and/or biofilm-associated infections represents a possibility that is increasingly taken into consideration. Over the last years, a growing body of research has focused on frog skin-derived AMPs with considerable attention being devoted to the antibacterial activity and the mechanism of action of TB (Conlon et al., 2014; Mangoni et al., 2016). It has emerged that such a peptide possesses significant membrane-perturbing properties and folds in a α-helix upon interaction with bacterial membranes (Mangoni et al., 2000). Like most of the members of the temporin family, TB is considerably effective against Gram-positive bacteria, including clinically important multidrug-resistant pathogens, but only poorly active against Gram-negative bacteria (Mangoni et al., 2008). The lower level of activity of TB against these bacteria is likely due to the presence of LPS that induces the oligomerization of the peptide, and hence prevents it to diffuse through the cell wall and reach the target cytoplasmic membrane (Rosenfeld et al., 2006; Mangoni and Shai, 2009). Design of TB analogs with modification of the peptide primary structure may provide peptides with stronger activity against Gram-negative bacterial species and increase the translational potential of TB. Computer-assisted design strategies have led us to obtain TB_L1FK, in which the leucine in position 1 has been replaced by a phenylalanine, the asparagine 7 has been eliminated and an extra lysine has been inserted at the C-terminus increasing the net charge of the peptide. Differently from the traditional optimization procedures, the computational method employed herein allowed to predict the effect of multiple amino acid positions on the antibacterial activity and cytotoxicity of TB, thereby enabling to improve different features of the peptide at the same time and to design a set of candidates for experimental validation. The other analog analyzed in this work, i.e., TB_KKG6A, has been designed by Avitabile and colleagues by replacing the glycine in position 6 with an alanine according to the Ala-scanning method and by adding two lysines at the N-terminus in order to produce a more cationic peptide (Avitabile et al., 2013). Circular dichroism and NMR studies have previously shown that TB_KKG6A strongly

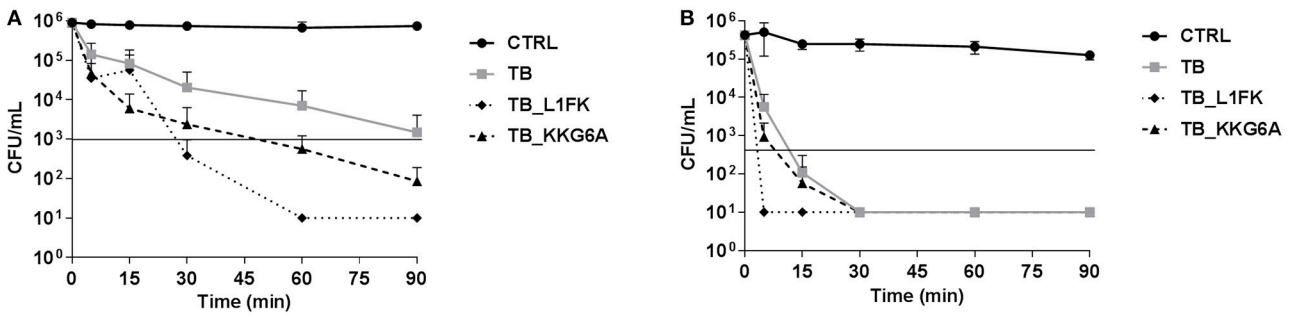

FIGURE 2 | Killing kinetics of TB, TB_L1FK, and TB_KKG6A against *S. aureus* ATCC 33591 (A) and *P. aeruginosa* ATCC 27853 **(B)**. Bacteria were incubated in sodium-phosphate buffer (10 mM SPB, pH 7.4) with the peptides at concentrations equal to their MBCs for various times. Control (CTRL) represents untreated bacteria. Solid line indicates a reduction of ≥3 Log_{10} in the number of control bacteria at each time of incubation. A number of 10 CFU/mL was taken as detection limit. Data are expressed as mean ± standard error of at least three independent experiments.

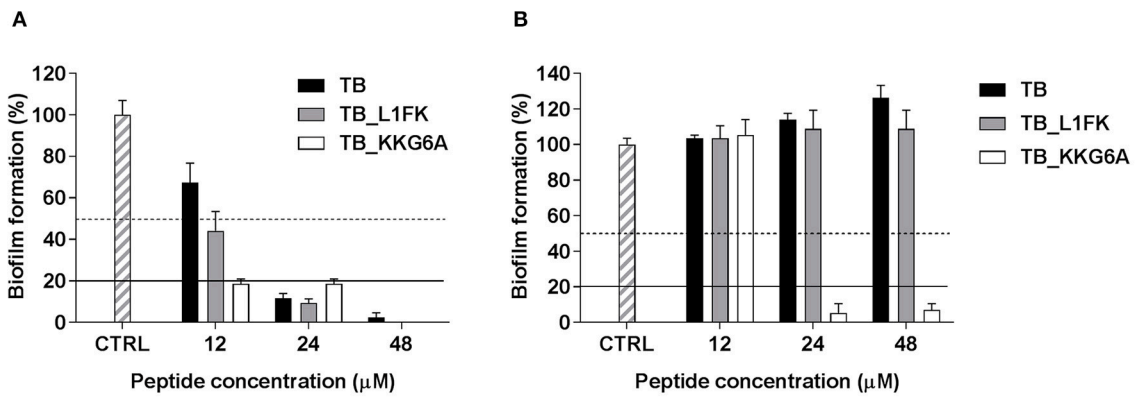

FIGURE 3 | Inhibitory effect of TB, TB_L1FK, and TB_KKG6A on biofilm formation of *S. aureus* ATCC 33591 (A) and *P. aeruginosa* ATCC 27853 **(B)**. The inhibitory effect was assessed by measuring the total biofilm biomass by crystal violet staining after 24 h of incubation with the peptides. Control (CTRL) represents untreated bacteria. Dashed and solid lines represent 50 and 80% reduction in biofilm biomass as compared to untreated controls, respectively. Data are reported as mean ± standard error of at least three independent experiments.

interacts with the LPS of the Gram-negative bacterium *E. coli* and assumes a bent helical conformation upon binding (Avitabile et al., 2013; Malgieri et al., 2015).

A comparative analysis of the properties of TB and these two analogs was performed starting from the evaluation of their bactericidal activity against multidrug-resistant bacteria in planktonic form. TB_L1FK and TB_KKG6A displayed an expanded spectrum of action as compared to the parental peptide, being active against all the tested Gram-positive and Gram-negative bacterial strains at very low concentrations. It is likely that the presence of additional positively charged amino acids in their sequence enhanced the affinity of the analogs toward Gram-negative bacteria. This observation is consistent with previous studies, in which optimized analogs of both TB and other temporins (Conlon et al., 2007; Capparelli et al., 2009; Srivastava and Ghosh, 2013) were obtained through the introduction of extra positive charges. Cationic amino acids, such as lysine, play a key role in the interaction of AMPs with the negatively charged components of the bacterial cell surface and the cytoplasmic membrane (Shai, 1999; Hancock and Sahl, 2006). Therefore, an increase in peptide cationicity can promote a more efficient interaction with bacteria, and hence a stronger antibacterial activity (Han et al., 2016). Moreover, faster killing kinetics were observed for the analogs compared to TB against both *S. aureus* and *P. aeruginosa*, selected as representative Gram-positive and Gram-negative bacterial species, respectively. The short time required for peptides to exert their bactericidal effect correlates with the bacterial membrane-permeabilizing activity of the temporin family (Mangoni et al., 2000; Saviello et al., 2010).

The three peptides were also compared regarding their antibiofilm properties using reference strains of *S. aureus* and *P. aeruginosa*. Biofilm-related infections currently represent a relevant clinical problem because of the intrinsic recalcitrance of biofilms to the antibiotic therapy. *S. aureus* and *P. aeruginosa* are common bacterial species involved in biofilm-associated infections, such as wound infections, lung infections in cystic fibrosis patients and implant-related infections (e.g., central venous catheters, endotracheal tubes, prostheses; Ciofu et al.,

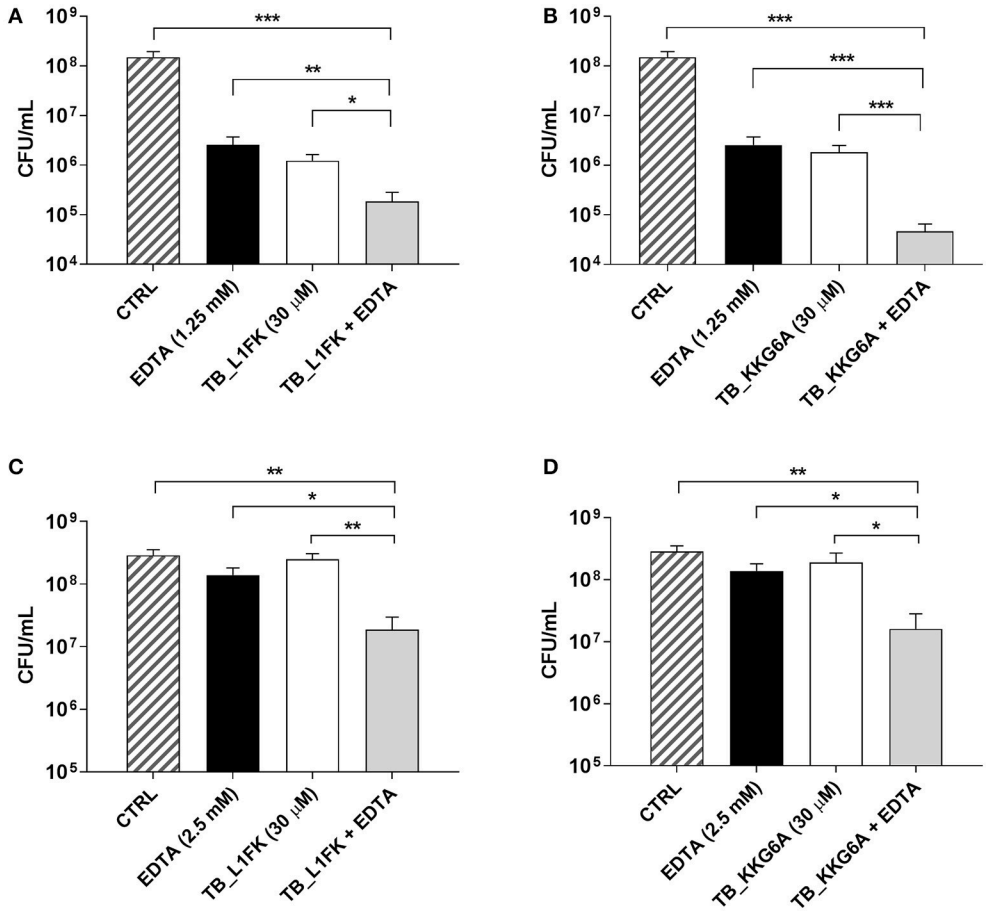

FIGURE 4 | Activity of TB_L1FK and TB_KKG6A, used alone and in combination with EDTA, against preformed (24-h old) biofilms of *S. aureus* ATCC 33591 (A,B) and *P. aeruginosa* ATCC 27853 **(C,D)**. The antibiofilm activity of the peptides, EDTA and the peptide-EDTA combinations was evaluated by CFU counting after 24 h of incubation. Control (CTRL) represents untreated biofilms. Data are reported as mean ± standard error of at least three independent experiments. $^{*}p < 0.05$; $^{**}p < 0.01$; $^{***}p < 0.001$ (one way ANOVA followed by Tukey-Kramer *post-hoc* test).

TABLE 3 | MICs of TB_L1FK and TB_KKG6A in biofilm-like conditions against *S. aureus* and *P. aeruginosa* and FIC index of the peptide-EDTA combinations.

	***S. aureus* ATCC 33591**		***P. aeruginosa* ATCC 27853**	
	TB_L1FK	**TB_KKG6A**	**TB_L1FK**	**TB_KKG6A**
MIC[a]	15	7.5	120	30
FIC index	>0.5	>0.5	0.25 (15 μM)[b]	0.25 (3.75 μM)

[a] *Concentrations are expressed in μM.*

[b] *Parentheses include the concentration of the peptide resulting in a synergistic effect.*

2015). The ability of these pathogens to produce biofilms is responsible for the establishment of chronic infections, thereby constituting a primary impediment to the complete recovery from infectious diseases (Costerton et al., 1999; Dean et al., 2011). Thus, the identification of new broad-spectrum antibiofilm agents and innovative therapeutic strategies appears as a growing need. To this aim, we explored the efficacy of TB and TB analogs both in preventing biofilm formation and in treating mature biofilms and attempted to enhance the antibiofilm activity of the peptides by combining them with adjuvant compounds. TB analogs showed an improved ability to inhibit the formation of *S. aureus* biofilms at 12 μM, while at 24 μM all three peptides were equally active, causing more than 80% reduction of the biofilm biomass. TB_KKG6A, but not TB_L1FK, showed also a marked activity in inhibiting biofilm formation of *P. aeruginosa* at the concentration of 24 μM. In all cases, the inhibitory activity of the peptides was observed at concentrations close to the MIC values determined in biofilm-like conditions (**Table 3**), suggesting that the antibiofilm effect was due to the direct killing of biofilm-forming bacteria at their planktonic stage rather than to biofilm-specific mechanisms (Segev-Zarko et al., 2015; Batoni et al., 2016a). When assayed against preformed biofilms, the two analogs, differently from TB, were able to significantly reduce the number of biofilm-associated cells of *S. aureus* at 30 μM, while none of the peptides was effective against *P. aeruginosa* even at 120 μM. It is commonly recognized that preformed biofilms are more challenging to target than the early stages of biofilm formation. The reduced susceptibility of mature biofilms

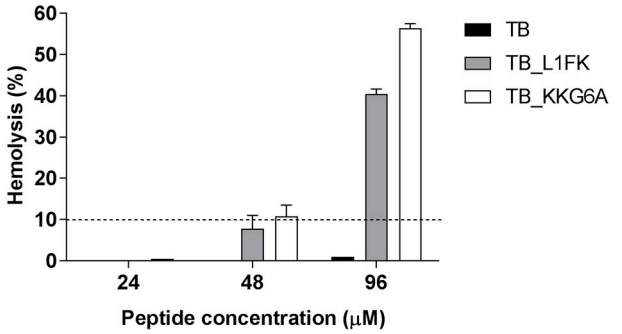

FIGURE 5 | Hemolytic activity of TB, TB_L1FK, and TB_KKG6A on human erythrocytes after 1 h of incubation at 37°C. The hemolytic activity was evaluated by the spectrophotometric determination of hemoglobin released from erythrocytes. PBS (0% hemolysis) and Triton X-100 (100% hemolysis) were used as controls. Hemolysis values ≤10% (dashed line) are considered to be non-hemolytic (Amin and Dannenfelser, 2006). Data are reported as mean ± standard error of three independent experiments.

to AMPs is mainly due to the presence of the extracellular matrix that surrounds the bacterial population and constitutes an actual impediment to peptide penetration into the biofilm structure (Otto, 2006; Batoni et al., 2016a). Cationic peptides can be repulsed or sequestrated by the biofilm extracellular polymeric molecules, especially exopolysaccharides and DNA, so that their interaction with bacterial cells can be significantly hampered (Batoni et al., 2016a). In particular, the polysaccharide intracellular adhesin (PIA) of staphylococcal biofilm matrix and alginate, Pel and Psl polysaccharides of *P. aeruginosa* biofilms have been demonstrated to play a major role in the protection from AMPs (Vuong et al., 2004; Chan et al., 2005). Thus, the use of AMPs in combination with compounds able to disaggregate the extracellular matrix could represent a promising strategy to increase their antibiofilm activity and therapeutic potential. In this regard, the chelator EDTA has been shown to reduce the structural integrity of the biofilm of several bacterial species by forming strong complexes with divalent cations (magnesium, calcium, iron) essential for matrix stability (Percival et al., 2005; Banin et al., 2006; Cavaliere et al., 2014; Maisetta et al., 2016). Herein, we combined TB analogs with EDTA in order to improve their efficacy against preformed biofilms of *S. aureus* and *P. aeruginosa*. The combination of TB_L1FK and TB_KKG6A with EDTA resulted in a potentiated antibiofilm effect that led to a statistically significant reduction in the viable count of both bacterial species at a peptide concentration of 30 μM. In order to prove that the enhancement of the antibiofilm activity of TB analogs was actually due to the destabilizing action of EDTA on the biofilm matrix, we also evaluated the effect of the combination peptide-EDTA on planktonic cells in biofilm-like conditions. Interestingly, the peptides exhibited synergy with EDTA against planktonic cultures of *P. aeruginosa*, but not against *S. aureus*. The combination treatment inhibited the growth of *P. aeruginosa* to a greater extent than the peptide used alone, suggesting a direct effect of EDTA also on planktonic bacteria. It is known that divalent cations are key elements in maintaining the integrity of the outer membrane of Gram-negative bacteria as they attenuate the electrostatic repulsive forces between adjacent LPS molecules by forming salt bridges (Gray and Wilkinson, 1965; Asbell and Eagon, 1966). Therefore, chelation of divalent cations by EDTA could enhance the action of the tested AMPs by destabilizing the outer membrane and thus facilitating the peptide access to the bacterial inner membrane. Furthermore, the chelating activity of EDTA may contribute to remove the cationic barrier that prevents the electrostatic interaction of cationic AMPs with the negatively charged bacterial surface (Walkenhorst et al., 2014). Thus, it is likely that EDTA mainly acted as an extracellular matrix-disaggregating agent in the case of *S. aureus* biofilms, facilitating the diffusion of the peptides through the biofilm layers. On the other hand, in the case of *P. aeruginosa* biofilms, the enhanced effect of the peptide-EDTA combinations could be very well due not only to the perturbing effect on the extracellular matrix, but also on a direct effect on biofilm-embedded cells.

The evaluation of the cytotoxicity of AMPs toward the host cells is an essential step to their development as therapeutics. It is generally accepted that there is a direct relationship between the antimicrobial potency of AMPs and their cytotoxic properties (Takahashi et al., 2010). A subtle balance of several physicochemical and structural parameters (cationicity, amphipathicity, hydrophobicity, and helicity) is necessary to ensure the maximum antibacterial efficacy and target cell selectivity of the peptides (Chen et al., 2005; Zelezetsky et al., 2005). Therefore, we evaluated the hemolytic effect of TB analogs on human erythrocytes and their cytotoxic activity on human PBMCs and the human-derived epithelial cell line A549. Along with the enhancement of the antimicrobial activity, modifications in TB sequence led to an overall increase of the hemolytic activity and cytotoxicity of the native peptide. Nevertheless, both TB_L1FK and TB_KKG6A were non-hemolytic at concentrations that resulted to be active against both planktonic and biofilm-growing bacteria. A percentage of hemolysis lower than 10% was assessed at peptide concentrations close to that used in combination with EDTA in treating mature biofilms of *S. aureus* and *P. aeruginosa*. When tested against mammalian cells, TB_L1FK resulted less cytotoxic than TB_KKG6A against human epithelial cells, suggesting that the computational method employed generated a sequence showing a good compromise between antibacterial and cytotoxic activity and promising features for topic applications. In the case of PBMCs, both TB analogs displayed comparable and quite high levels of cytotoxicity. A promising solution to reduce the toxicity of AMPs is the development of appropriate delivery systems for their controlled and/or targeted release. In this regard, our group has recently developed a chitosan-based nanostructured delivery system loaded with TB that ensured a considerable reduction of the cytotoxic activity of the peptide toward mammalian cells (Piras et al., 2015).

CONCLUSIONS

In the present study, we performed a detailed characterization of the bactericidal and antibiofilm activity of TB analogs in

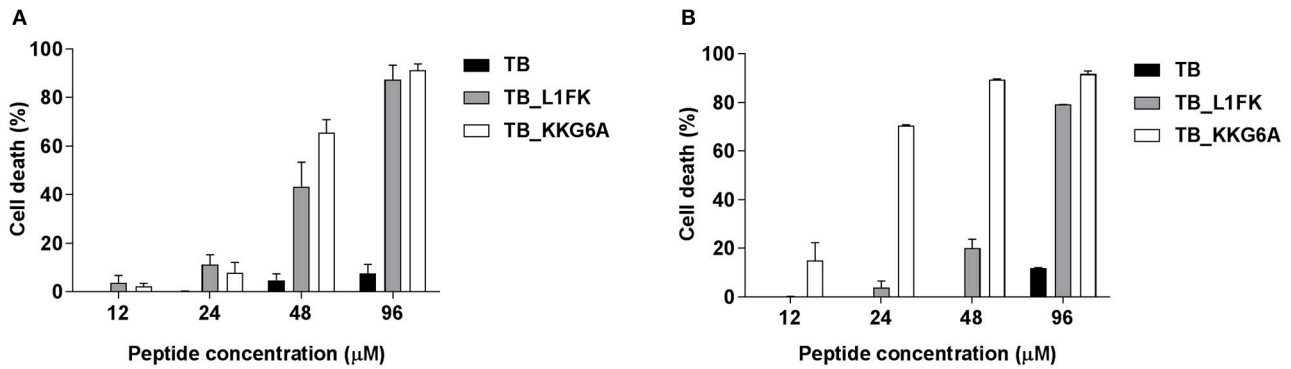

FIGURE 6 | Cytotoxicity of TB, TB_L1FK, and TB_KKG6A on human PBMCs (A) and A549 cells **(B)** after 24 h of incubation at 37°C, 5% CO_2. The cytotoxic activity was evaluated by the PI flow cytometric assay. Cells incubated with culture medium only (100% cell viability) and cells treated with cycloheximide (0% cell viability) were used as controls. Data are reported as mean ± standard error of three independent experiments.

order to demonstrate the potential of computational peptide design in the improvement of the antimicrobial properties of AMPs. The introduction of appropriate modifications in the primary sequence of TB led to optimized analogs with a stronger and faster bactericidal activity and a wider spectrum of action as compared to the parental peptide. Furthermore, TB analogs exhibited an improved ability both in preventing biofilm formation and in treating preformed biofilms of *S. aureus* and *P. aeruginosa*, especially when used in combination with EDTA. The antibiofilm action of the peptide-EDTA combination was likely due to a disaggregating effect on the biofilm extracellular matrix and/or to a direct effect on bacterial cells. Collectively, our results suggest that TB analogs represent a promising template for the development of novel antimicrobials for the treatment of antibiotic-resistant and/or biofilm-associated infections. In this regard, current work is devoted to the development of a nanostructured delivery system for TB analogs with the aim to reduce their toxicity and to control their pharmacokinetics, thus further improving the therapeutic potential of these molecules.

AUTHOR CONTRIBUTIONS

LG, GAM, SE, and GB: conception and design of the work; acquisition, analysis, and interpretation of the data for the work; GM: design and analysis of TB_L1FK; LG, GAM, GM, and GB: drafting of the work; LG, GAM, GM, SE, and GB: critical revision of the work; final approval.

FUNDING

This work was supported by funds from University of Pisa (Rating di Ateneo).

SUPPLEMENTARY MATERIAL

The Supplementary Material for this article can be found online at: http://journal.frontiersin.org/article/10.3389/fchem.2017.00024/full#supplementary-material

REFERENCES

Amin, K., and Dannenfelser, R. (2006). *In vitro* hemolysis: guidance for the pharmaceutical scientist. *J. Pharm. Sci.* 95, 1173–1176. doi: 10.1002/jps.20627

Asbell, M. A., and Eagon, R. G. (1966). Role of multivalent cations in the organization, structure, and assembly of the cell wall of *Pseudomonas aeruginosa*. *J. Bacteriol.* 92, 380–387.

Avitabile, C., Netti, F., Orefice, G., Palmieri, M., Nocerino, N., Malgieri, G., et al. (2013). Design, structural and functional characterization of a Temporin-1b analog active against Gram-negative bacteria. *Biochim. Biophys. Acta* 1830, 3767–3775. doi: 10.1016/j.bbagen.2013.01.026

Banin, E., Brady, K. P., and Greenberg, E. P. (2006). Chelator-induced dispersal of *Pseudomonas aeruginosa* cells in a biofilm. *Appl. Environ. Microbiol.* 72, 2064–2069. doi: 10.1128/AEM.72.3.2064-2069.2006

Batoni, G., Casu, M., Giuliani, A., Luca, V., Maisetta, G., Mangoni, M. L., et al. (2016b). Rational modification of a dendrimeric peptide with antimicrobial activity: consequences on membrane-binding and biological properties. *Amino Acids* 48, 887–900. doi: 10.1007/s00726-015-2136-5

Batoni, G., Maisetta, G., and Esin, S. (2016a). Antimicrobial peptides and their interaction with biofilms of medically relevant bacteria. *Biochim. Biophys. Acta* 1858, 1044–1060. doi: 10.1016/j.bbamem.2015.10.013

Boucher, H. W., Talbot, G. H., Bradley, J. S., Edwards, J. E., Gilbert, D., Rice, L. B., et al. (2009). Bad bugs, no drugs: no ESKAPE! An update from the infectious diseases society of America. *Clin. Infect. Dis.* 48, 1–12. doi: 10.1086/595011

Capparelli, R., Romanelli, A., Iannaccone, M., Nocerino, N., Ripa, R., Pensato, S., et al. (2009). Synergistic antibacterial and anti-inflammatory activity of temporin A and modified temporin B *in vivo*. *PLoS ONE* 4:e7191. doi: 10.1371/journal.pone.0007191

Cavaliere, R., Ball, J. L., Turnbull, L., and Whitchurch, C. B. (2014). The biofilm matrix destabilizers, EDTA and DNase I, enhance the susceptibility of nontypeable *Hemophilus influenzae* biofilms to treatment with ampicillin and ciprofloxacin. *Microbiologyopen* 3, 557–567. doi: 10.1002/mbo3.187

Chan, C., Burrows, L. L., and Deber, C. M. (2005). Alginate as an auxiliary bacterial membrane: binding of membrane-active peptides by polysaccharides. *J. Pept. Res.* 65, 343–351. doi: 10.1111/j.1399-3011.2005.00217.x

Chen, Y., Mant, C. T., Farmer, S. W., Hancock, R. E., Vasil, M. L., and Hodges, R. S. (2005). Rational design of alpha-helical antimicrobial peptides with enhanced activities and specificity/therapeutic index. *J. Biol. Chem.* 280, 12316–12329. doi: 10.1074/jbc.M413406200

Ciofu, O., Tolker-Nielsen, T., Jensen, P. Ø, Wang, H., and Høiby, N. (2015). Antimicrobial resistance, respiratory tract infections and role of biofilms in lung infections in cystic fibrosis patients. *Adv. Drug Deliv. Rev.* 85, 7–23. doi: 10.1016/j.addr.2014.11.017

Conlon, J. M., Al-Ghaferi, N., Abraham, B., and Leprince, J. (2007). Strategies for transformation of naturally-occurring amphibian antimicrobial peptides into therapeutically valuable anti-infective agents. *Methods* 42, 349–357. doi: 10.1016/j.ymeth.2007.01.004

Conlon, J. M., Mechkarska, M., Lukic, M. L., and Flatt, P. R. (2014). Potential therapeutic applications of multifunctional host-defense peptides from frog skin as anti-cancer, anti-viral, immunomodulatory and anti-diabetic agents. *Peptides* 57C, 67–77. doi: 10.1016/j.peptides.2014.04.019

Costerton, J. W., Stewart, P. S., and Greenberg, E. P. (1999). Bacterial biofilms: a common cause of persistent infections. *Science* 284, 1318–1322. doi: 10.1126/science.284.5418.1318

Dean, S. N., Bishop, B. M., and van Hoek, M. L. (2011). Susceptibility of *Pseudomonas aeruginosa* biofilm to alpha-helical peptides: D-enantiomer of LL-37. *Front. Microbiol.* 2:128. doi: 10.3389/fmicb.2011.00128

Di Grazia, A., Luca, V., Segev-Zarko, L. T., Shai, Y., and Mangoni, M. L. (2014). Temporins A and B stimulate migration of HaCaT keratinocytes and kill intracellular *Staphylococcus aureus*. *Antimicrob. Agents Chemother.* 58, 2520–2527. doi: 10.1128/AAC.02801-13

Di Luca, M., Maccari, G., Maisetta, G., and Batoni, G. (2015). BaAMPs: the database of biofilm-active antimicrobial peptides. *Biofouling* 31, 193–199. doi: 10.1080/08927014.2015.1021340

Di Luca, M., Maccari, G., and Nifosì, R. (2014). Treatment of microbial biofilms in the post-antibiotic era: prophylactic and therapeutic use antimicrobial and their design by bioinformatics tools. *Pathog. Dis.* 70, 257–270. doi: 10.1111/2049-632X.12151

Dosler, S., Karaaslan, E., and Alev Gerceker, A. (2016). Antibacterial and anti-biofilm activities of mellitin and colistin, alone and in combination with antibiotics against Gram-negative bacteria. *J. Chemother.* 28, 95–103. doi: 10.1179/1973947815Y.0000000004

Gray, G. W., and Wilkinson, S. G. (1965). The effect of ethylendiaminetetraacetic acid on the cell walls of some gram-negative bacteria. *J. Gen. Microbiol.* 39, 385–399.

Gupta, S., Kapoor, P., Chaudhary, K., Gautam, A., Kumar, R., and Raghava, G. P. (2013). *In silico* approach for predicting toxicity of peptides and proteins. *PLoS ONE* 8:e73957. doi: 10.1371/journal.pone.0073957

Han, H. M., Gopal, M., and Park, Y. (2016). Design and membrane-disruption mechanism of charge-enriched AMPs exhibiting cell selectivity, high-salt resistance, and anti-biofilm properties. *Amino Acids* 48, 505–522. doi: 10.1007/s00726-015-2104-0

Hancock, R. E., and Sahl, H. G. (2006). Antimicrobial and host-defense peptides as new anti-infective therapeutic strategies. *Nat. Biotechnol.* 24, 1551–1556. doi: 10.1038/nbt1267

Högberg, L. D., Heddini, A., and Cars, O. (2010). The global need for effective antibiotics: challenges and recent advances. *Trends Pharmacol. Sci.* 31, 509–515. doi: 10.1016/j.tips.2010.08.002

Høiby, N., Bjarnsholt, T., Givskov, M., Molin, S., and Ciofu, O. (2010). Antibiotic resistance of bacterial biofilms. *Int. J. Antimicrob. Agents* 35, 322–332. doi: 10.1016/j.ijantimicag.2009.12.011

Katragkou, A., McCarthy, M., Alexander, E. L., Antachopoulos, C., Meletiadis, J., Jabra-Rizk, M. A., et al. (2015). *In vitro* interactions between farnesol and fluconazole, amphotericin B or micafungin against *Candida albicans* biofilms. *J. Antimicrob. Chemother.* 70, 470–478. doi: 10.1093/jac/dku374

Lamiable, A., Thévenet, P., Rey, J., Vavrusa, M., Derreumaux, P., and Tufféry, P. (2016). PEP-FOLD3: faster *denovo* structure prediction for linear peptides in solution and in complex. *Nucleic Acid Res.* 44, 449–454. doi: 10.1093/nar/gkw329

Maccari, G., Di Luca, M., Nifosí, R., Cardarelli, F., Signore, G., Boccardi, C., et al. (2013). Antimicrobial peptides design by evolutionary multiobjective optimization. *PLoS Comput. Biol.* 9:e1003212. doi: 10.1371/journal.pcbi.1003212

Maisetta, G., Grassi, L., Di Luca, M., Bombardelli, S., Medici, C., Brancatisano, F. L., et al. (2016). Anti-biofilm properties of the antimicrobial peptide Temporin 1Tb and its ability, in combination with EDTA, to eradicate *Staphylococcus epidermidis* biofilms on silicone catheters. *Biofouling* 32, 787–800. doi: 10.1080/08927014.2016.1194401

Malgieri, G., Avitabile, C., Palmieri, M., D'Andrea, L. D., Isernia, C., Romanelli, A., et al. (2015). Structural basis of a temporin 1b analogue antimicrobial activity against Gram-negative bacteria determined by CD and NMR techniques in cellular environment. *ACS Chem. Biol.* 10, 965–969. doi: 10.1021/cb501057d

Mangoni, M. L., Grazia, A. D., Cappiello, F., Casciaro, B., and Luca, V. (2016). Naturally occurring peptides from *Rana temporaria*: antimicrobial properties and more. *Curr. Top. Med. Chem.* 16, 54–64. doi: 10.2174/1568026615666150703121403

Mangoni, M. L., Maisetta, G., Di Luca, M., Gaddi, L. M., Esin, S., Florio, W., et al. (2008). Comparative analysis of the bactericidal activities of amphibian peptide analogues against multidrug-resistant nosocomial bacterial strains. *Antimicrob. Agents Chemother.* 52, 85–91. doi: 10.1128/AAC.00796-07

Mangoni, M. L., Rinaldi, A. C., Di Giulio, A., Mignogna, G., Bozzi, A., Barra, D., et al. (2000). Structure-function relationships of temporins, small antimicrobial peptides from amphibian skin. *Eur. J. Biochem.* 267, 1447–1454. doi: 10.1046/j.1432-1327.2000.01143.x

Mangoni, M. L., and Shai, Y. (2009). Temporins and their synergism against Gram-negative bacteria and in lypopolysaccharide detoxification. *Biochim. Biophys. Acta.* 1788, 1610–1619. doi: 10.1016/j.bbamem.2009.04.021

Otto, M. (2006). Bacterial evasion of antimicrobial peptides by biofilm formation. *Curr. Top. Microbiol. Immunol.* 306, 251–258. doi: 10.1007/3-540-29916-5_10

Percival, S. L., Kite, P., Eastwood, K., Murga, R., Carr, J., Arduino, M. J., et al. (2005). Tetrasodium EDTA as a novel central venous catheter lock solution against biofilm. *Infect. Control Hosp. Epidemiol.* 26, 515–519. doi: 10.1086/502577

Piras, A. M., Maisetta, G., Sandreschi, S., Gazzarri, M., Bartoli, C., Grassi, L., et al. (2015). Chitosan nanoparticles loaded with the antimicrobial peptide temporin B exert a long-term antibacterial activity *in vitro* against clinical isolated of *Staphylococcus epidermidis*. *Front Microbiol.* 6:372. doi: 10.3389/fmicb.2015.00372

Rosenfeld, Y., Barra, M., Simmaco, M., Shai, Y., and Mangoni, M. L. (2006). A synergism between temporins towards Gram-negative bacteria overcomes resistance imposed by the lypopolysaccharide protective layer. *J. Biol. Chem.* 281, 28565–28574. doi: 10.1074/jbc.M606031200

Saviello, M. R., Malfi, S., Campiglia, P., Cavalli, A., Grieco, P., Novellino, E., et al. (2010). New insight into the mechanism of action of the temporin antimicrobial peptides. *Biochemistry* 49, 1477–1485. doi: 10.1021/bi902166d

Segev-Zarko, L., Saar-Dover, R., Brumfeld, V., Mangoni, M. L., and Shai, Y. (2015). Mechanism of biofilm inhibition and degradation by antimicrobial peptides. *Biochem. J.* 468, 259–270. doi: 10.1042/BJ20141251

Shai, Y. (1999). Mechanism of the binding, insertion and destabilization of phospholipid bilayer membranes by alpha-helical antimicrobial and cell non-selective membrane-lytic peptides. *Biochim. Biophys. Acta* 1462, 55–70. doi: 10.1016/S0005-2736(99)00200-X

Srivastava, S., and Ghosh, J. K. (2013). Introduction of a lysine residue promotes aggregation of temporin L in lipopolysaccharides and augmentation of its antiendotoxin property. *Antimicrob. Agents Chemother.* 57, 2457–2466. doi: 10.1128/AAC.00169-13

Takahashi, D., Shukla, S. K., Prakash, O., and Zhang, G. (2010). Structural determinants of host defence peptides for antimicrobial activity and target cell selectivity. *Biochimie* 92, 1236–1241. doi: 10.1016/j.biochi.2010.02.023

Tavanti, A., Maisetta, G., Del Gaudio, G., Petruzzelli, R., Sanguinetti, M., Batoni, G., et al. (2011). Fungicidal activity of the human peptide hepcidin 20 alone or in combination with other antifungals against *Candida glabrata* isolates. *Peptides* 32, 2484–2487. doi: 10.1016/j.peptides.2011.10.012

Vuong, C., Voyich, J. M., Fisher, E. R., Braughton, K. R., Whitney, A. R., DeLeo, F. R., et al. (2004). Polysaccharide intercellular adhesin (PIA) protects *Staphylococcus epidermidis* against major components of the human innate immune system. *Cell. Microbiol.* 6, 269–275. doi: 10.1046/j.1462-5822.2004.00367.x

Walkenhorst, W. F., Sundrud, J. N., and Laviolette, J. M. (2014). Additivity and synergy between an antimicrobial peptide and inhibitory ions. *Biochim. Biophys. Acta* 1838, 2234–2242. doi: 10.1016/j.bbamem.2014.05.005

Zasloff, M. (2002). Antimicrobial peptides of multicellular organisms. *Nature* 415, 389–395. doi: 10.1038/415389a

Zelezetsky, I., Pacor, S., Pag, U., Papo, N., Shai, Y., Sahl, H. G., et al. (2005). Controlled alteration of the shape and conformational stability of alpha-helical cell-lytic peptides: effect on mode of action and cell specificity. *Biochem. J.* 390, 177–188. doi: 10.1042/BJ20042138

Conflict of Interest Statement: The authors declare that the research was conducted in the absence of any commercial or financial relationships that could be construed as a potential conflict of interest.

Supplementary Material:

Analogues of the Frog-skin Antimicrobial Peptide Temporin 1Tb Exhibit a Wider Spectrum of Activity and a Stronger Antibiofilm Potential as Compared to the Parental Peptide

Lucia Grassi, Giuseppantonio Maisetta, Giuseppe Maccari, Semih Esin, Giovanna Batoni *

***Correspondence:**
Giovanna Batoni
giovanna.batoni@med.unipi.it

1 SUPPLEMENTARY DATA

1.1 Dataset preparation

A dataset representing peptides with cytotoxic activity was designed with the aim to train and validate a statistical model able to discern between 'toxic' and 'non-toxic' peptides, giving a confidence score. A set of sequences ranging from 9 to 35 amino acids length was collected from different bioactive peptide databases, as previously described (Gupta et al, 2013). After removal of peptides with non-standard residues, 1709 peptides were left. The negative dataset was populated with non-secretory sequences randomly extracted from UniProt database, without the 'antimicrobic' and 'cytotoxic' annotation and with a length ranging from 9 to 35 amino acids, for a total count of 2010 negative sequences. A homology cut-off was imposed to exclude similar peptides in order to avoid redundant data that could influence the prediction performance. Peptides showing a sequence identity equal or greater than 70% to any other in the dataset were identified and removed by the CD-HIT (Cluster Database at High Identity with Tolerance) program (Li and Godzik, 2006).

1.2 Data encoding

In order to build a statistical model, able to discern between toxic and non-toxic peptides, each sequence in the dataset was encoded into computer-intelligible variables representing peptides physicochemical peculiarities. Peptide charge at different pH conditions, isoelectric point and molecular weight, together with the z-scale moment, were used to describe global features of the peptide sequences. Z-scale descriptors (Hellberg et al, 1987) are highly condensed variables, originally derived from a principal component analysis (PCA) of several experimental and theoretical physicochemical properties for the 20 naturally occurring amino acids (AAs). These descriptors were successively expanded to include artificial AAs for a total of 87 AAs (Sandberg et al, 1998). In detail, this latter version corresponds to the first five principal components explaining the variance in the set: z_1, z_2, and z_3 represent the AA hydrophobicity, steric properties, and polarity, respectively, while z_4 and z_5 describe the electronic effects of the residues. The z-scale moment (μZ_i), an extension of Eisenberg's hydrophobic moment equation (Eisenberg at al, 1982), represents z-scales distribution along peptide sequences.

$$\mu Z_i = \sqrt{\left(\sum_{k=1}^{L} Z_i^k \sin(\delta k)\right)^2 + \left(\sum_{k=1}^{L} Z_i^k \cos(\delta k)\right)^2}$$

Equation 1. Z-scale moment

In Equation 1, δ is the angular frequency of the AA residues forming the structure (100° for alpha helix); k is the number of the particular residue examined, L is the length of the sequence and Z_i^k is the z_i-scale value of the k^{th} AA. In particular, μZ_1 represents a measure of the hydrophobicity distribution along peptide sequence. Topological descriptors represent the interaction of different residues along the amino acidic sequence and are used to keep into account peptide's secondary structure. QSAR descriptors were encoded into auto- and cross covariance (ACC) values. Classical ACC transformation was introduced by Wold et al. (Wold et al, 1993) and results in two kinds of variables: auto covariance (AC) of the same descriptor and cross covariance (CC) between two different descriptors. Briefly, for a given protein sequence, ACC variables describe the average interactions between residues distributed a certain *lag* apart throughout the whole sequence. In this work, the *Minimum and Maximum of auto- and cross-covariances* (mMACC) algorithm is used (Maccari et al, 2013), weak and strong correlations are kept into account (Equation 2).

$$AC_{\min d} = MIN\left[Z_i^k * Z_i^{k+d}\right]; AC_{\max d} = MAX\left[Z_i^k * Z_i^{k+d}\right](k = 1,2,3..L-d)$$
$$CC_{\min d} = MIN\left[Z_i^k * Z_i^{k+d}\right]; CC_{\max d} = MAX\left[Z_i^k * Z_i^{k+d}\right](k = 1,2,3..L-d)$$

Equation 2. Minimum and Maximum of auto and cross-covariance equations

Both in the global and topological descriptors, Z-scale values were mean-centered and scaled prior to their use, as described by the following equation:

$$Z_i = \frac{z_i - \frac{1}{N}\sum_{k=1}^{N} z_i^k}{\sqrt{\frac{1}{N}\sum_{j=1}^{N}\left[z_i^j - \frac{1}{N}\sum_{k=1}^{N} z_i^k\right]^2}}$$

Equation 3. Z-scale descriptor normalization

Where Z_i is the i^{th} descriptor of z-scales variables, z_i is the original z-scale value and N is the number of AAs in the z-scales descriptors table.

1.3 Feature selection and model generation

In this study, the Random Forest algorithm (RF), implemented in the software suite WEKA (Witten et al, 2011), was adopted as prediction engine. Model performance was measured with a 10-fold cross-validation analysis, where each dataset was divided into 10 parts - 9 parts for model learning (training) and the remaining part for validation (testing). As a performance measure, the Matthews correlation coefficient (MCC) was used, as defined below.

$$\text{Sensitivity} = \frac{TP}{TP + FN}$$

$$\text{Precision} = \frac{TP}{TP + FP}$$

$$\text{Accuracy} = \frac{TP + TN}{TP + TN + FP + FN}$$

$$MCC = \frac{(TP * TN) - (FN * FP)}{\sqrt{(TP + FN) * (TN + FP) * (TP + FP) * (TN + FN)}}$$

Equation 4. Performance evaluation equations

Where *TP*, *TN*, *FP* and *FN* are the number of true positive, true negative, false positive and false negative, respectively, resulting from the model. MCC is an important index used to evaluate the performance of the predictor when the dataset is not balanced (Baldi et al, 2000). In order to obtain a non-redundant set of descriptors, the Maximum Relevance, Minimum Redundancy (mRMR) method (Peng et al, 2005) was employed to sort features in descending order of importance. Incremental Feature Selection (IFS) (Huang et al, 2010) was applied to the sorted descriptors list by consecutively incrementing by 5 the number of descriptors. Each descriptor set thus obtained was evaluated by tenfold cross-validation and the IFS curve was plotted to unveil the relation between the performance of the model and the feature subset. The optimal feature subset is defined as that showing the highest MCC value (**Figure S1**); the selected model was used for peptides classification. A description of the applied descriptors is available in **Table S1**, while the hierarchical list of the final descriptors is shown in **Table S2**.

1.4 Sequence similarity

For TB peptide optimization, a supplemental objective representing sequence similarity was added. Sequence similarity is defined by the Smith-Waterman score between the respective peptide sequences (Smith at al, 1981). However, since the Smith-Waterman score is dependent on input sequences length, the final score was normalized between 0 and 1 by dividing by the maximum score of the two self-alignments, as shown in Equation 5 (Zang et al, 2012).

$$NS_{A,B} = \frac{S_{A,B}}{\max\left(S_{A,A}, S_{B,B}\right)}$$

Equation 5. Smith-Waterman normalized score

Here, $S_{A,B}$ is the similarity score between sequence A and B, $S_{A,A}$ and $S_{B,B}$ are the self-alignment score of sequence A and sequence B, respectively. In order to consider not only the identity between two amino acidic positions, a score matrix was defined by calculating the Euclidean distance between the five auto-scaled z-scale values of each AA pairs.

References

Baldi P., Brunak S., Chauvin Y., Andersen C.A.F., Nielsen H. (2000). Assessing the accuracy of prediction algorithms for classification: an overview. *Bioinformatics.* 16: 412-424.

Eisenberg D., Weiss R.M.,. Terwilliger T.C. (1982). The helical hydrophobic moment: a measure of the amphiphilicity of a helix. *Nature* 299: 371-374.

Gupta, S., Kapoor, P., Chaudhary, K., Gautam, A., Kumar, R., Raghava, G.P.S. (2013). In silico approach for predicting toxicity of peptides and proteins. *PLoS One.* 8:e73957. doi: 10.1371/journal.pone.0073957.

Hellberg S., Sjöström M., Skagerberg B., Wold S. (1987). Peptide quantitative structure activity relationship, a multivariate approach. *J. Med. Chem*. 30: 1126-1135.

Huang T., Shi X.H., Wang P., He Z., Feng K.Y., Hu L., Kong X., Li Y.X., Cai Y.D., Chou K.C. (2010). Analysis and prediction of the metabolic stability of proteins based on their sequential features, subcellular locations and interaction networks. *PLoS One.* 5: e10972.

Li, W., Godzik, A. (2006). Cd-hit: a fast program for clustering and comparing large sets of protein or nucleotide sequences. *Bioinformatics.* 22: 1658-1659. doi: 10.1093/bioinformatics/btl158.

Maccari G., Di Luca M., Nifosí R., Cardarelli F., Signore G., Boccardi C., Bifone A. (2013). Antimicrobial peptides design by evolutionary multiobjective optimization. *PLoS Comput Biol.* 9: e1003212.

Peng H., Long F., Ding C. (2005). Feature selection based on mutual information: criteria of max-dependency, max-relevance, and min-redundancy. *IEEE Trans. Pattern Anal. Mach. Intell.* 27: 1226-1238.

Sandberg M., Eriksson L., Jonsson J., Sjöström M., Wold S. (1998). New chemical descriptors relevant for the design of biologically active peptides. A multivariate characterization of 87 amino acids. *J. Med. Chem*. 41: 2481-2491.

Smith T.F., Waterman M.S. (1981). Identification of common molecular subsequences. *J. Mol. Biol.* 147: 195–197.

Witten I.H., Frank E., Hall M.A. (2011). Data mining: practical machine learning tools and techniques. Morgan Kaufmann, Burlington, MA

Wold S., Jonsson J., Sjöström M., Sandberg M., Rännar S. (1993). DNA and peptide sequences and chemical processes multivariately modelled by principal component analysis and partial least-squares projections to latent structures. *Ann. Chim. Acta*. 277: 239-253.

Zang M., Leong H. (2012). BBH-LS: an algorithm for computing positional homologs using sequence and gene context similarity. *BMC Syst. Biol.* 6: S22.

2 SUPPLEMENTARY TABLES AND FIGURES

2.1 Tables

Table S1. Applied descriptors in the model building. A list of the applied descriptors with abbreviation and description is provided.

Type	Abbreviation	Description
Global	NetCharge@5	Net charge at pH = 5.
	NetCharge@7	Net charge at pH = 7.
	NetCharge@9	Net charge at pH = 9.
	Wimley White (pH n)	Wimley White partitioning at pH *n*
	Isoelectric point	Peptide's isoelectric point
	Size	Total amino acid count.
	Property_Zn	Z-scale average sum of property *n* along peptide sequence.
	Variable Moment Z*n* (100 D)	Z-scale moment distribution of property n along peptide sequence at 100 degrees (the angle between two residues in alpha helix conformation)
Topological	D_X_AC_LAG_N_[MIN,MAX]; D_X:Y_CC_LAG_N_[MIN,MAX]	D_X_AC_LAG_N_[MIN,MAX]: Topological descriptor of the auto covariance of descriptor X with a lag of N. D_X:Y_CC_LAG_N_[MIN,MAX]: Topological descriptor of the cross covariance between descriptor X and Y, with a lag of N. With X and Y being a value between 0 and 4: 0) Z-scale Descriptor 1 1) Z-scale Descriptor 2 2) Z-scale Descriptor 3 3) Z-scale Descriptor 4 4) Z-scale Descriptor 5

Table S2. Hierarchical list of descriptors. List of descriptors sorted by the mRMR method.

	Name	#	Name	#	Name	#	Name	#	Name	#	Name
		11	D_4:0_CC_LAG_3_	23		34		46		57	D_4:3_CC_LAG_1_
2	Property_z5_10	7	MIN	2	D_0:2_CC_LAG_5_MIN	7	D_1:3_CC_LAG_5_MIN	2	D_1:0_CC_LAG_7_MAX	7	MIN
		11	D_0:1_CC_LAG_4_	23		34		46		57	D_3:1_CC_LAG_9_
3	Property_z2_6	8	MIN	3	D_0:4_CC_LAG_5_MIN	8	D_1_AC_LAG_4_MIN	3	D_2:1_CC_LAG_3_MAX	8	MAX
		11		23		34		46		57	
4	Property_z3_14	9	Property_z2_12	4	D_0:4_CC_LAG_8_MAX	9	D_2:0_CC_LAG_7_MIN	4	D_0_AC_LAG_8_MIN	9	Property_z3_20
		12		23		35		46		58	D_2:3_CC_LAG_0_
5	Property_z2_2	0	Property_z3_16	5	D_1:0_CC_LAG_4_MIN	0	D_0_AC_LAG_6_MIN	5	D_3:1_CC_LAG_1_MAX	0	MAX
		12	D_4_AC_LAG_0_MI	23		35		46		58	D_2:3_CC_LAG_5_
6	Property_z5_9	1	N	6	D_2:1_CC_LAG_3_MIN	1	D_2:1_CC_LAG_6_MAX	6	D_4:3_CC_LAG_8_MIN	1	MIN
		12	D_0:2_CC_LAG_0_	23		35		46		58	
7	Property_z2_3	2	MIN	7	D_4_AC_LAG_6_MAX	2	D_0:2_CC_LAG_8_MIN	7	Property_z1_31	2	Property_z1_29
		12	D_1:0_CC_LAG_1_	23		35		46		58	D_1:2_CC_LAG_2_
8	Property_z2_1	3	MIN	8	D_3:0_CC_LAG_3_MAX	3	D_4:0_CC_LAG_9_MIN	8	D_3_AC_LAG_4_MAX	3	MAX
		12	D_4:1_CC_LAG_6_	23		35		46		58	D_2:1_CC_LAG_9_
9	Property_z5_6	4	MAX	9	D_0:3_CC_LAG_4_MIN	4	D_1:0_CC_LAG_2_MAX	9	D_4:2_CC_LAG_9_MAX	4	MAX
		12		24		35		47		58	D_4:3_CC_LAG_4_
10	Property_z4_5	5	Property_z4_34	0	D_1:4_CC_LAG_3_MIN	5	D_2:0_CC_LAG_3_MAX	0	D_1_AC_LAG_5_MAX	5	MIN
		12	D_0:4_CC_LAG_1_	24		35		47		58	D_2:4_CC_LAG_8_
11	Property_z2_34	6	MAX	1	D_1:3_CC_LAG_3_MAX	6	D_3:1_CC_LAG_9_MIN	1	D_3:2_CC_LAG_5_MIN	6	MIN
		12	D_2:1_CC_LAG_2_	24		35		47		58	
12	Property_z2_9	7	MIN	2	D_4_AC_LAG_4_MAX	7	D_3_AC_LAG_0_MIN	2	Property_z2_16	7	Property_z2_18
		12	D_0:4_CC_LAG_1_	24		35		47		58	D_4:2_CC_LAG_0_
13	Property_z2_7	8	MIN	3	Property_z5_14	8	D_0_AC_LAG_7_MAX	3	D_2:1_CC_LAG_9_MIN	8	MIN
		12	D_3:0_CC_LAG_1_	24		35		47		58	D_3:2_CC_LAG_3_
14	Property_z1_4	9	MAX	4	D_0:2_CC_LAG_8_MAX	9	D_1:4_CC_LAG_5_MIN	4	D_1_AC_LAG_6_MAX	9	MAX
		13		24		36		47		59	
15	Property_z2_11	0	Property_z5_12	5	Property_z5_33	0	Property_z5_32	5	D_3:4_CC_LAG_2_MIN	0	Property_z2_29
		13	D_4:0_CC_LAG_7_	24		36		47		59	
16	Property_z3_1	1	MAX	6	D_0:1_CC_LAG_3_MAX	1	D_2:0_CC_LAG_6_MIN	6	D_3_AC_LAG_8_MAX	1	Property_z3_22
	D_1:2_CC_LAG_3_MI	13		24		36		47		59	D_0:2_CC_LAG_7_
17	N	2	Property_z4_0	7	D_0:1_CC_LAG_7_MIN	2	D_1:2_CC_LAG_0_MAX	7	D_1:2_CC_LAG_8_MAX	2	MAX
		13	D_0:1_CC_LAG_0_	24		36		47		59	D_4:2_CC_LAG_5_
18	Property_z1_9	3	MIN	8	D_0_AC_LAG_1_MIN	3	D_3:2_CC_LAG_0_MIN	8	Property_z2_31	3	MIN
		13	D_4:1_CC_LAG_1_	24		36		47		59	D_2:4_CC_LAG_5_
19	Property_z3_3	4	MAX	9	D_4:3_CC_LAG_7_MAX	4	D_1:4_CC_LAG_9_MAX	9	D_1:3_CC_LAG_8_MAX	4	MIN
		13	D_4:1_CC_LAG_1_	25		36		48		59	
20	Property_z2_10	5	MIN	0	D_3:1_CC_LAG_2_MIN	5	D_1:3_CC_LAG_3_MIN	0	D_2:1_CC_LAG_8_MAX	5	Property_z3_21
		13		25		36		48		59	D_3:4_CC_LAG_5_
21	Property_z1_2	6	Property_z2_13	1	D_0:2_CC_LAG_4_MIN	6	D_0:3_CC_LAG_8_MIN	1	D_2:3_CC_LAG_9_MIN	6	MIN
		13	D_3:0_CC_LAG_4_	25		36		48		59	D_2:0_CC_LAG_0_
22	Property_z2_8	7	MIN	2	D_3_AC_LAG_7_MIN	7	D_0:1_CC_LAG_8_MAX	2	D_4:2_CC_LAG_5_MAX	7	MAX

		13	D_0:4_CC_LAG_7_	25		36		48	Wimley-White Partitioning	59	D_2:4_CC_LAG_2_
23	Property_z4_4	8	MAX	3	D_4:0_CC_LAG_4_MIN	8	D_0_AC_LAG_5_MIN	3	(pH9.0)	8	MIN
		13	D_3:4_CC_LAG_0_	25		36		48		59	
24	Property_z3_12	9	MAX	4	D_1:4_CC_LAG_7_MAX	9	D_4:3_CC_LAG_6_MIN	4	D_3:2_CC_LAG_7_MIN	9	Property_z3_26
	Variable moment	14	D_4_AC_LAG_1_M	25		37		48		60	D_0:2_CC_LAG_6_
25	(z2:100.0D)	0	AX	5	D_0:3_CC_LAG_4_MAX	0	D_3:1_CC_LAG_7_MIN	5	Property_z3_28	0	MAX
		14	D_0_AC_LAG_3_MI	25		37		48		60	D_3:2_CC_LAG_0_
26	Property_z2_0	1	N	6	D_0:1_CC_LAG_1_MIN	1	D_3_AC_LAG_7_MAX	6	D_3_AC_LAG_3_MAX	1	MAX
		14	D_1:3_CC_LAG_8_	25		37		48		60	
27	Property_z1_8	2	MIN	7	D_1:4_CC_LAG_6_MIN	2	D_1_AC_LAG_3_MIN	7	D_1:0_CC_LAG_6_MAX	2	Property_z4_16
		14	D_4:0_CC_LAG_1_	25		37		48		60	D_4:3_CC_LAG_3_
28	Property_z3_7	3	MIN	8	D_4_AC_LAG_0_MAX	3	D_1:2_CC_LAG_5_MAX	8	D_2:0_CC_LAG_7_MAX	3	MIN
		14		25		37		48		60	
29	D_4_AC_LAG_5_MIN	4	Property_z3_34	9	D_0:1_CC_LAG_2_MAX	4	NetCharge@5.0	9	Property_z5_16	4	Property_z3_25
		14	D_2:1_CC_LAG_4_	26		37		49		60	D_2:4_CC_LAG_7_
30	Property_z1_5	5	MIN	0	D_0:2_CC_LAG_6_MIN	5	D_4:1_CC_LAG_9_MAX	0	D_2:3_CC_LAG_3_MIN	5	MIN
		14	D_4:3_CC_LAG_3_	26		37		49		60	D_3:2_CC_LAG_5_
31	Property_z3_2	6	MAX	1	D_4:3_CC_LAG_5_MIN	6	Property_z4_32	1	D_3:0_CC_LAG_8_MAX	6	MAX
		14	D_4:3_CC_LAG_0_	26		37		49		60	D_2:3_CC_LAG_9_
32	Property_z1_11	7	MAX	2	D_4:0_CC_LAG_8_MIN	7	D_3:0_CC_LAG_5_MAX	2	D_3:4_CC_LAG_8_MIN	7	MAX
		14	D_3:0_CC_LAG_5_	26		37		49		60	D_2:3_CC_LAG_4_
33	Property_z5_7	8	MIN	3	D_0_AC_LAG_4_MAX	8	D_1:3_CC_LAG_6_MIN	3	D_1_AC_LAG_9_MIN	8	MAX
		14	D_4:0_CC_LAG_4_	26		37		49		60	
34	Property_z3_0	9	MAX	4	D_2:0_CC_LAG_2_MIN	9	D_0:1_CC_LAG_9_MIN	4	D_3:1_CC_LAG_6_MAX	9	Property_z2_19
		15		26		38		49		61	D_2:4_CC_LAG_1_
35	Property_z5_1	0	Property_z1_17	5	D_3:1_CC_LAG_8_MIN	0	D_4:2_CC_LAG_0_MAX	5	Property_z4_30	0	MIN
		15	D_0:2_CC_LAG_3_	26		38		49		61	D_3:4_CC_LAG_3_
36	Property_z3_9	1	MIN	6	Property_z4_33	1	D_0_AC_LAG_4_MIN	6	D_4:3_CC_LAG_7_MIN	1	MIN
		15	D_1_AC_LAG_0_M	26		38		49		61	
37	Property_z5_11	2	AX	7	D_3:4_CC_LAG_2_MAX	2	D_1:3_CC_LAG_4_MAX	7	D_3:2_CC_LAG_6_MIN	2	Property_z1_28
	D_4:1_CC_LAG_0_MA	15	D_4_AC_LAG_2_M	26		38		49		61	D_3:2_CC_LAG_6_
38	X	3	AX	8	D_1:2_CC_LAG_7_MIN	3	D_3:0_CC_LAG_6_MAX	8	D_2:1_CC_LAG_4_MAX	3	MAX
		15	D_1:0_CC_LAG_3_	26		38		49		61	D_4:2_CC_LAG_6_
39	Property_z5_2	4	MIN	9	D_0:1_CC_LAG_0_MAX	4	D_4:2_CC_LAG_8_MIN	9	Property_z1_22	4	MIN
	Variable moment	15	D_1:4_CC_LAG_1_	27		38		50		61	
40	(z3:100.0D)	5	MIN	0	D_4:1_CC_LAG_2_MIN	5	Property_z5_15	0	D_1_AC_LAG_8_MAX	5	Property_z1_23
	D_4:0_CC_LAG_1_MA	15		27		38		50		61	D_3:2_CC_LAG_8_
41	X	6	Property_z2_14	1	D_2:4_CC_LAG_4_MAX	6	D_1_AC_LAG_1_MAX	1	D_1:2_CC_LAG_1_MAX	6	MAX
		15	D_0:3_CC_LAG_1_	27		38		50		61	D_2:4_CC_LAG_0_
42	Property_z5_8	7	MAX	2	D_4_AC_LAG_1_MIN	7	D_2:1_CC_LAG_7_MAX	2	D_3_AC_LAG_4_MIN	7	MIN
		15	D_4:0_CC_LAG_0_	27		38		50		61	D_3:2_CC_LAG_7_
43	Property_z1_13	8	MAX	3	D_3:4_CC_LAG_7_MAX	8	D_2:0_CC_LAG_8_MIN	3	Property_z5_18	8	MAX
	D_0:4_CC_LAG_3_MI	15		27		38		50		61	
44	N	9	Property_z5_34	4	D_0:1_CC_LAG_5_MAX	9	D_0_AC_LAG_1_MAX	4	D_2:3_CC_LAG_6_MIN	9	Property_z5_28
	D_2:0_CC_LAG_0_MI	16	D_0:3_CC_LAG_2_	27		39		50		62	D_2:0_CC_LAG_2_
45	N	0	MIN	5	D_0:3_CC_LAG_3_MIN	0	D_1:4_CC_LAG_4_MIN	5	D_4:2_CC_LAG_3_MAX	0	MAX
		16	D_4:0_CC_LAG_5_	27		39		50		62	D_2:4_CC_LAG_4_
46	Property_z4_12	1	MAX	6	NetCharge@7.0	1	D_1:3_CC_LAG_7_MAX	6	D_1_AC_LAG_5_MIN	1	MIN

		16	D_2:0_CC_LAG_1_	27		39		50		62	
47	Property_z1_1	2	MIN	7	D_1:3_CC_LAG_7_MIN	2	D_3:1_CC_LAG_3_MIN	7	Property_z5_30	2	Property_z4_17
		16	D_1:0_CC_LAG_8_	27		39		50		62	
48	Property_z3_8	3	MIN	8	D_4_AC_LAG_8_MIN	3	D_1:3_CC_LAG_5_MAX	8	Property_z1_20	3	Property_z2_24
	D_3:1_CC_LAG_4_MI	16	D_4_AC_LAG_8_M	27		39		50		62	D_3:4_CC_LAG_4_
49	N	4	AX	9	D_1:0_CC_LAG_0_MAX	4	D_1:2_CC_LAG_9_MIN	9	D_3:2_CC_LAG_8_MIN	4	MIN
	D_4:3_CC_LAG_4_MA	16	D_3:1_CC_LAG_1_	28		39		51		62	D_0:2_CC_LAG_1_
50	X	5	MIN	0	D_0:4_CC_LAG_6_MIN	5	D_0:3_CC_LAG_8_MAX	0	D_2:3_CC_LAG_8_MAX	5	MAX
	D_3:0_CC_LAG_0_MI	16	D_1_AC_LAG_2_MI	28		39		51		62	
51	N	6	N	1	D_4_AC_LAG_2_MIN	6	D_4:2_CC_LAG_6_MAX	1	D_1_AC_LAG_6_MIN	6	Property_z2_28
	Variable moment	16	D_4:0_CC_LAG_6_	28		39		51		62	D_4:2_CC_LAG_8_
52	(z1:100.0D)	7	MIN	2	D_2:1_CC_LAG_6_MIN	7	D_3:1_CC_LAG_5_MAX	2	D_2:4_CC_LAG_6_MAX	7	MAX
		16	D_4:3_CC_LAG_2_	28		39		51		62	D_2:4_CC_LAG_3_
53	Property_z3_10	8	MAX	3	D_1_AC_LAG_1_MIN	8	D_0:2_CC_LAG_9_MIN	3	D_3_AC_LAG_3_MIN	8	MIN
		16	D_0:4_CC_LAG_3_	28		39		51		62	D_2:0_CC_LAG_1_
54	Property_z4_6	9	MAX	4	D_0_AC_LAG_3_MAX	9	D_3:0_CC_LAG_7_MAX	4	Property_z1_19	9	MAX
		17	D_0:2_CC_LAG_2_	28		40		51		63	
55	Property_z2_5	0	MIN	5	D_3:0_CC_LAG_8_MIN	0	D_4:1_CC_LAG_8_MIN	5	D_0:2_CC_LAG_0_MAX	0	Property_z2_21
		17	D_0:1_CC_LAG_5_	28		40		51		63	D_3:4_CC_LAG_0_
56	Property_z4_11	1	MIN	6	Property_z1_32	1	D_3:1_CC_LAG_2_MAX	6	D_2:3_CC_LAG_0_MIN	1	MIN
		17	D_4:0_CC_LAG_2_	28		40		51		63	
57	Property_z1_3	2	MIN	7	D_2:4_CC_LAG_1_MAX	2	D_2:4_CC_LAG_9_MAX	7	D_1:3_CC_LAG_9_MAX	2	Property_z4_28
	Variable moment	17	D_3:0_CC_LAG_0_	28		40		51		63	D_2:3_CC_LAG_2_
58	(z4:100.0D)	3	MAX	8	D_2:1_CC_LAG_0_MIN	3	D_0_AC_LAG_8_MAX	8	Property_z2_30	3	MAX
	D_0:4_CC_LAG_2_MA	17	D_0:4_CC_LAG_4_	28		40		51		63	
59	X	4	MAX	9	D_1:3_CC_LAG_2_MAX	4	D_0:4_CC_LAG_9_MIN	9	D_3_AC_LAG_8_MIN	4	Property_z2_23
		17	D_1:0_CC_LAG_2_	29		40		52		63	D_3:2_CC_LAG_9_
60	Property_z2_4	5	MIN	0	D_0:4_CC_LAG_9_MAX	5	D_1:0_CC_LAG_4_MAX	0	D_3:4_CC_LAG_9_MIN	5	MAX
		17	D_1:4_CC_LAG_2_	29		40		52		63	D_0:2_CC_LAG_5_
61	Property_z4_7	6	MAX	1	D_4:0_CC_LAG_7_MIN	6	D_1:3_CC_LAG_0_MAX	1	D_4:2_CC_LAG_9_MIN	6	MAX
	D_1:2_CC_LAG_0_MI	17	D_4:3_CC_LAG_2_	29		40		52		63	D_2:3_CC_LAG_1_
62	N	7	MIN	2	D_4:1_CC_LAG_7_MIN	7	D_1:4_CC_LAG_8_MIN	2	Property_z3_18	7	MAX
	D_1:0_CC_LAG_5_MI	17	D_4_AC_LAG_7_MI	29		40		52		63	
63	N	8	N	3	D_3:4_CC_LAG_5_MAX	8	D_3:2_CC_LAG_4_MIN	3	D_2:4_CC_LAG_2_MAX	8	Property_z2_22
		17	D_0_AC_LAG_2_MI	29		40		52		63	D_3:4_CC_LAG_1_
64	Property_z1_12	9	N	4	D_1:2_CC_LAG_8_MIN	9	D_0:3_CC_LAG_9_MIN	4	D_4:2_CC_LAG_1_MIN	9	MIN
		18	D_2:1_CC_LAG_7_	29		41		52		64	
65	Property_z4_2	0	MIN	5	D_4_AC_LAG_7_MAX	0	D_2:4_CC_LAG_0_MAX	5	D_2:0_CC_LAG_9_MAX	0	Property_z3_24
	D_1:4_CC_LAG_1_MA	18	D_4:1_CC_LAG_5_	29		41		52		64	D_2:3_CC_LAG_3_
66	X	1	MAX	6	D_4:1_CC_LAG_8_MAX	1	D_1_AC_LAG_7_MIN	6	Property_z3_23	1	MAX
		18	D_3:0_CC_LAG_6_	29		41		52		64	
67	Property_z3_13	2	MIN	7	D_0:4_CC_LAG_7_MIN	2	Property_z1_18	7	D_1_AC_LAG_9_MAX	2	Property_z4_27
		18	D_1:4_CC_LAG_0_	29	Wimley-White Partitioning	41		52		64	D_2_AC_LAG_9_MI
68	Property_z4_9	3	MIN	8	(pH5.0)	3	D_3:1_CC_LAG_0_MAX	8	D_3:2_CC_LAG_4_MAX	3	N
	Variable moment	18	D_3:4_CC_LAG_1_	29		41		52		64	
69	(z5:100.0D)	4	MAX	9	D_4_AC_LAG_3_MIN	4	D_2:3_CC_LAG_8_MIN	9	D_2:3_CC_LAG_7_MIN	4	Property_z2_20
		18	D_1:2_CC_LAG_6_	30		41		53		64	
70	Property_z4_1	5	MIN	0	D_1:3_CC_LAG_1_MIN	5	D_0:3_CC_LAG_9_MAX	0	D_3_AC_LAG_2_MAX	5	Property_z5_27

		18	D_4_AC_LAG_3_M	30		41		53		64	D_0:2_CC_LAG_2_
71	Property_z4_10	6	AX	1	D_1:4_CC_LAG_8_MAX	6	Property_z5_31	1	D_1_AC_LAG_8_MIN	6	MAX
	D_4:0_CC_LAG_6_MA	18	D_0:3_CC_LAG_5_	30		41		53		64	D_2_AC_LAG_9_M
72	X	7	MIN	2	D_1:2_CC_LAG_2_MIN	7	D_4:1_CC_LAG_6_MIN	2	Property_z1_30	7	AX
	D_0:3_CC_LAG_2_MA	18	D_4:3_CC_LAG_8_	30		41		53		64	
73	X	8	MAX	3	D_4:0_CC_LAG_9_MAX	8	D_4:2_CC_LAG_7_MAX	3	D_2:0_CC_LAG_6_MAX	8	Property_z2_27
		18	D_1:4_CC_LAG_5_	30		41		53		64	
74	Property_z4_8	9	MAX	4	D_2:0_CC_LAG_4_MIN	9	D_3:1_CC_LAG_8_MAX	4	Property_z2_17	9	Property_z1_27
		19		30		42		53		65	D_2_AC_LAG_5_MI
75	Property_z1_6	0	Property_z5_13	5	D_0:4_CC_LAG_4_MIN	0	D_1:3_CC_LAG_9_MIN	5	D_3:2_CC_LAG_9_MIN	0	N
		19	D_0:4_CC_LAG_0_	30		42		53		65	D_2_AC_LAG_3_M
76	Property_z5_5	1	MAX	6	D_0_AC_LAG_0_MAX	1	D_3:4_CC_LAG_9_MAX	6	D_1:2_CC_LAG_7_MAX	1	AX
	D_3:0_CC_LAG_1_MI	19	D_1:3_CC_LAG_0_	30		42		53		65	D_2_AC_LAG_5_M
77	N	2	MIN	7	D_3_AC_LAG_1_MIN	2	D_1:3_CC_LAG_1_MAX	7	D_3_AC_LAG_9_MIN	2	AX
		19		30		42		53		65	
78	Property_z1_0	3	Property_z1_33	8	D_0:3_CC_LAG_6_MIN	3	D_2:1_CC_LAG_5_MAX	8	D_2:3_CC_LAG_7_MAX	3	Property_z1_26
		19	D_0:3_CC_LAG_3_	30		42		53		65	D_2_AC_LAG_0_M
79	D_4_AC_LAG_4_MIN	4	MAX	9	D_2:4_CC_LAG_5_MAX	4	D_0:1_CC_LAG_7_MAX	9	D_2:3_CC_LAG_1_MIN	4	AX
		19	D_1:0_CC_LAG_7_	31		42		54		65	
80	Property_z4_3	5	MIN	0	D_1:4_CC_LAG_6_MAX	5	D_0:4_CC_LAG_8_MIN	0	D_2:4_CC_LAG_7_MAX	5	Property_z4_26
	D_0:4_CC_LAG_2_MI	19	D_4:1_CC_LAG_3_	31		42		54		65	D_2_AC_LAG_3_MI
81	N	6	MAX	1	D_1:3_CC_LAG_4_MIN	6	D_1:2_CC_LAG_4_MAX	1	Property_z5_19	6	N
	D_1:4_CC_LAG_4_MA	19	D_4:0_CC_LAG_2_	31		42		54		65	D_2_AC_LAG_0_MI
82	X	7	MAX	2	D_0:3_CC_LAG_7_MAX	7	D_0_AC_LAG_9_MIN	2	D_1:0_CC_LAG_9_MAX	7	N
		19	D_4:0_CC_LAG_0_	31		42		54		65	
83	Property_z5_4	8	MIN	3	D_0:2_CC_LAG_7_MIN	8	D_3_AC_LAG_1_MAX	3	D_4:3_CC_LAG_0_MIN	8	Property_z5_26
		19	D_2:0_CC_LAG_3_	31		42		54		65	D_2_AC_LAG_4_M
84	Property_z1_34	9	MIN	4	D_0_AC_LAG_2_MAX	9	D_4:1_CC_LAG_4_MIN	4	D_3:2_CC_LAG_2_MIN	9	AX
		20		31		43		54		66	
85	Property_z1_14	0	Property_z1_16	5	D_4_AC_LAG_9_MIN	0	D_1_AC_LAG_4_MAX	5	Property_z3_27	0	Property_z4_18
		20	D_0:3_CC_LAG_0_	31		43		54		66	D_2_AC_LAG_4_MI
86	NetCharge@9.0	1	MAX	6	D_0:1_CC_LAG_1_MAX	1	D_2:0_CC_LAG_9_MIN	6	D_2:1_CC_LAG_2_MAX	1	N
		20	D_4:1_CC_LAG_3_	31		43		54		66	
87	Property_z5_3	2	MIN	7	D_3:4_CC_LAG_6_MIN	2	D_3:1_CC_LAG_7_MAX	7	D_2:3_CC_LAG_2_MIN	2	Property_z2_26
	D_1:0_CC_LAG_0_MI	20	D_4_AC_LAG_9_M	31		43		54		66	D_2_AC_LAG_6_MI
88	N	3	AX	8	D_1:0_CC_LAG_9_MIN	3	Property_z4_31	8	D_2:0_CC_LAG_5_MAX	3	N
	D_3:0_CC_LAG_2_MA	20	D_0_AC_LAG_6_M	31		43		54		66	D_2_AC_LAG_6_M
89	X	4	AX	9	D_3_AC_LAG_6_MAX	4	D_4:2_CC_LAG_2_MAX	9	Property_z3_19	4	AX
		20	D_0:1_CC_LAG_6_	32		43		55		66	
90	Property_z3_11	5	MIN	0	D_3:1_CC_LAG_6_MIN	5	D_1:0_CC_LAG_5_MAX	0	D_3_AC_LAG_2_MIN	5	Property_z1_24
		20	D_4:0_CC_LAG_5_	32		43		55		66	D_2_AC_LAG_8_MI
91	Property_z1_10	6	MIN	1	Property_z3_32	6	D_0:1_CC_LAG_6_MAX	1	D_1:2_CC_LAG_9_MAX	6	N
		20	D_2:1_CC_LAG_1_	32		43		55		66	
92	Property_z5_0	7	MIN	2	D_1:0_CC_LAG_3_MAX	7	D_4:1_CC_LAG_5_MIN	2	Property_z3_30	7	Property_z4_25
	D_4:0_CC_LAG_3_MA	20	D_4:1_CC_LAG_4_	32		43		55		66	
93	X	8	MAX	3	D_2:1_CC_LAG_5_MIN	8	D_1_AC_LAG_3_MAX	3	D_3:4_CC_LAG_7_MIN	8	Property_z4_19
	D_0:3_CC_LAG_0_MI	20	D_2:4_CC_LAG_3_	32		43		55		66	D_2_AC_LAG_7_M
94	N	9	MAX	4	D_4:3_CC_LAG_9_MAX	9	Property_z3_17	4	D_2:3_CC_LAG_4_MIN	9	AX

		21	D_3:0_CC_LAG_3_	32		44		55		67	
95	Property_z3_6	0	MIN	5	D_1:4_CC_LAG_7_MIN	0	D_3_AC_LAG_6_MIN	5	D_3_AC_LAG_9_MAX	0	Property_z5_25
	D_1:4_CC_LAG_0_MA	21	D_1:2_CC_LAG_5_	32		44		55		67	D_2_AC_LAG_8_M
96	X	1	MIN	6	D_0:1_CC_LAG_8_MIN	1	D_0_AC_LAG_7_MIN	6	Property_z1_21	1	AX
	D_0:1_CC_LAG_3_MI	21		32		44		55		67	D_2_AC_LAG_7_MI
97	N	2	Property_z1_15	7	D_0:1_CC_LAG_4_MAX	2	D_3:2_CC_LAG_2_MAX	7	D_0:2_CC_LAG_3_MAX	2	N
		21		32		44		55		67	
98	Property_z1_7	3	Isoelectric point	8	D_3:4_CC_LAG_8_MAX	3	D_0:1_CC_LAG_9_MAX	8	D_4:2_CC_LAG_7_MIN	3	Property_z2_25
	D_0:4_CC_LAG_6_MA	21	D_3:4_CC_LAG_4_	32		44		55		67	D_2_AC_LAG_1_M
99	X	4	MAX	9	D_2:0_CC_LAG_8_MAX	4	D_1:4_CC_LAG_9_MIN	9	D_2:1_CC_LAG_1_MAX	4	AX
10	D_0:4_CC_LAG_0_MI	21	D_0:1_CC_LAG_2_	33		44		56		67	
0	N	5	MIN	0	D_2:0_CC_LAG_5_MIN	5	D_3:1_CC_LAG_4_MAX	0	D_3:0_CC_LAG_9_MAX	5	Property_z4_24
10		21	D_4:0_CC_LAG_8_	33		44		56		67	D_2_AC_LAG_2_M
1	Property_z3_15	6	MAX	1	D_0:3_CC_LAG_6_MAX	6	D_3:2_CC_LAG_1_MIN	1	D_4:3_CC_LAG_9_MIN	6	AX
10	D_1:2_CC_LAG_4_MI	21	D_1_AC_LAG_7_M	33		44		56		67	
2	N	7	AX	2	D_1_AC_LAG_0_MIN	7	D_2:0_CC_LAG_4_MAX	2	D_4:2_CC_LAG_3_MIN	7	Property_z4_20
10	D_0:4_CC_LAG_5_MA	21	D_1:3_CC_LAG_2_	33		44		56		67	
3	X	8	MIN	3	D_3:1_CC_LAG_5_MIN	8	D_1:0_CC_LAG_8_MAX	3	D_3:2_CC_LAG_1_MAX	8	Property_z5_24
10		21		33		44		56		67	D_2_AC_LAG_1_MI
4	Property_z4_13	9	Property_z3_33	4	D_1:2_CC_LAG_6_MAX	9	Property_z3_31	4	Property_z5_17	9	N
10		22	D_1:0_CC_LAG_1_	33		45		56		68	D_2_AC_LAG_2_MI
5	Property_z3_4	0	MAX	5	D_1_AC_LAG_2_MAX	0	D_3_AC_LAG_5_MIN	5	D_1:2_CC_LAG_3_MAX	0	N
10	D_4:1_CC_LAG_2_MA	22	D_4:3_CC_LAG_6_	33		45		56		68	
6	X	1	MAX	6	Property_z2_15	1	D_2:1_CC_LAG_8_MIN	6	Property_z5_29	1	Property_z5_23
10		22		33		45		56		68	
7	Property_z2_33	2	Property_z4_14	7	D_0_AC_LAG_9_MAX	2	D_2:4_CC_LAG_8_MAX	7	D_2:3_CC_LAG_6_MAX	2	Property_z4_23
10	D_0:3_CC_LAG_1_MI	22	D_1:4_CC_LAG_3_	33		45		56		68	
8	N	3	MAX	8	D_3_AC_LAG_5_MAX	3	D_3:1_CC_LAG_3_MAX	8	D_4:2_CC_LAG_4_MIN	3	Property_z1_25
10	D_4:1_CC_LAG_0_MI	22	D_0_AC_LAG_5_M	33		45	Wimley-White Partitioning	56		68	
9	N	4	AX	9	D_1:4_CC_LAG_2_MIN	4	(pH7.0)	9	D_2:4_CC_LAG_6_MIN	4	Property_z4_21
11		22	D_3:0_CC_LAG_7_	34		45		57		68	
0	D_4_AC_LAG_6_MIN	5	MIN	0	Property_z2_32	5	D_3_AC_LAG_0_MAX	0	D_0:2_CC_LAG_4_MAX	5	Property_z4_22
11	D_0:2_CC_LAG_1_MI	22	D_4_AC_LAG_5_M	34		45		57		68	
1	N	6	AX	1	D_1:2_CC_LAG_1_MIN	6	D_4:1_CC_LAG_9_MIN	1	Property_z5_20	6	Molecular Weight
11	D_4:3_CC_LAG_5_MA	22	D_4:3_CC_LAG_1_	34		45		57		68	
2	X	7	MAX	2	D_4:2_CC_LAG_4_MAX	7	D_4:2_CC_LAG_1_MAX	2	D_2:3_CC_LAG_5_MAX	7	Property_z5_22
11	D_1:0_CC_LAG_6_MI	22	D_2:1_CC_LAG_0_	34		45		57		68	
3	N	8	MAX	3	D_3:0_CC_LAG_9_MIN	8	D_1:3_CC_LAG_6_MAX	3	D_2:4_CC_LAG_9_MIN	8	Size
11		22	D_3:1_CC_LAG_0_	34		45		57		68	
4	D_0_AC_LAG_0_MIN	9	MIN	4	D_3:0_CC_LAG_4_MAX	9	Property_z3_29	4	D_0:2_CC_LAG_9_MAX	9	Property_z5_21
11		23	D_4:1_CC_LAG_7_	34		46		57			
5	Property_z3_5	0	MAX	5	D_0:3_CC_LAG_7_MIN	0	D_3:2_CC_LAG_3_MIN	5	Property_z4_29		
11	D_3:4_CC_LAG_3_MA	23	D_3:4_CC_LAG_6_	34		46		57			
6	X	1	MAX	6	D_0:3_CC_LAG_5_MAX	1	Property_z4_15	6	D_4:2_CC_LAG_2_MIN		

2.2 Figures

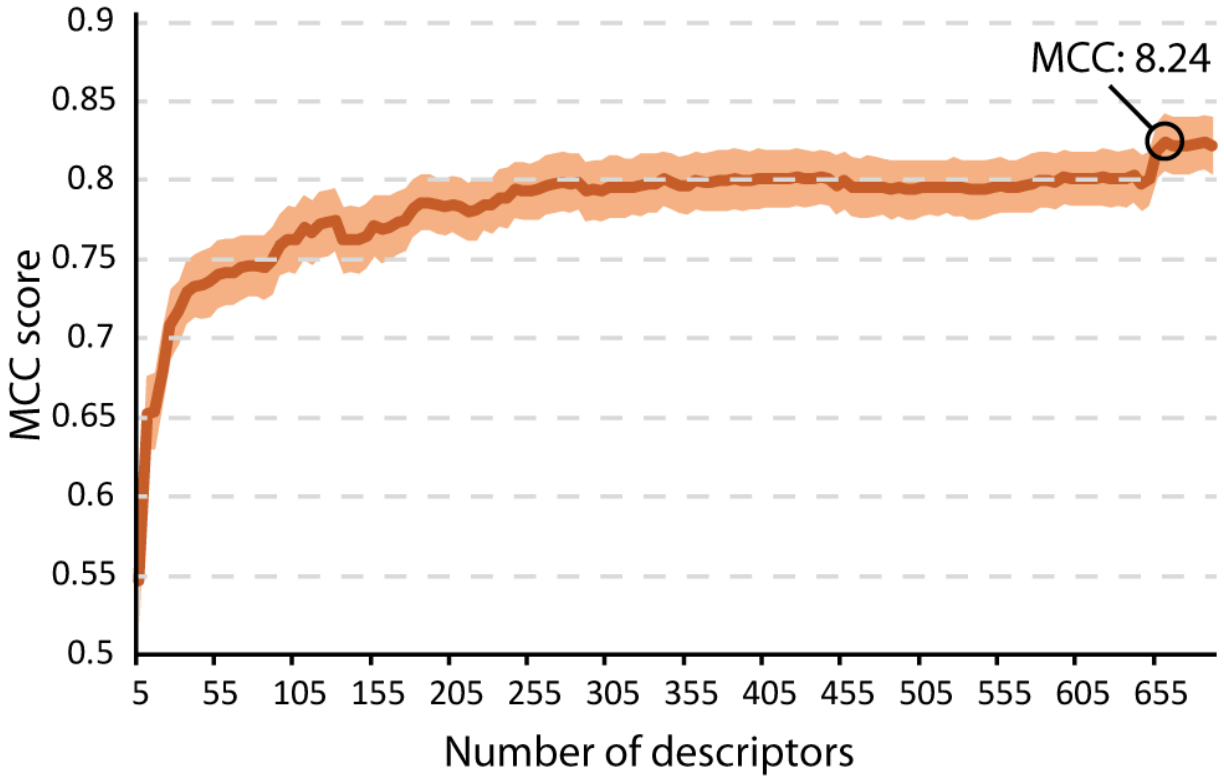

Figure S1. IFS results. Ten-fold cross validation of the sorted list of descriptors. The descriptor list was sorted by Maximum Relevance, Minimum Reduncancy (mRMR) and a total number of 138 models were trained. The model giving the highest MCC score was selected.